Aus dem Berliner Institut für Gesundheitsforschung (BIH)
– Abteilung Digitale Medizin –
der Medizinischen Fakultät Charité – Universitätsmedizin Berlin

DISSERTATION

Modellierung der Invasion von Glioblastomen mittels Mikroskopie und Sequenzierung

Combined imaging and sequencing to model glioblastoma invasion

zur Erlangung des akademischen Grades
Doctor medicinae (Dr. med.)

vorgelegt der Medizinischen Fakultät
Charité – Universitätsmedizin Berlin

von

Teresa Gabriela Krieger

aus Fulda

Datum der Promotion: 25. November 2022

Content

Abstract

Glioblastoma (GBM) is the most frequent and most aggressive primary adult brain tumour, with an expected survival time of only 12-15 months from diagnosis and a 5-year survival rate of 5%. Despite intensive research, treatment outcomes for GBM have barely improved over the past decades. Invasion of tumour cells into the surrounding brain tissue and significant genetic and transcriptional heterogeneity have impeded therapeutic progress.

In the work presented here, we harness recent advances in organoid generation and single-cell sequencing technologies to establish an experimental model system of glioblastoma invasion into brain organoids. We establish human brain organoids from induced pluripotent stem cells (iPSCs) and co-culture them with fluorescently labelled patient-derived GBM cells. Tumour cells invade into organoids within three days and extend membrane-bound microtubes that are up to 450 μm long, mirroring the formation of GBM cell networks previously observed *in vivo*. Invasion is visualised and quantified by tissue clearing and confocal microscopy. Our model is highly scalable and reproducible, enabling the study of the invasion process on clinically relevant timescales of less than one month in high-throughput applications.

Single-cell transcriptomics analyses of GBM cells before and after co-culture with organoid cells reveal substantial interpatient heterogeneity, but also identify transcriptional changes that are consistent across patients and may thus be generally implicated in the interactions of tumour cells with normal brain cells. Novel treatment strategies targeting tumour invasion and microtube formation could therefore provide clinical benefit to GBM patients in the future.

Together, these results demonstrate the utility of our experimental system for modelling glioblastoma invasion *in vitro* to improve our understanding of glioblastoma biology, as well as our ability to develop targeted therapies and select personalised treatment approaches for this as yet uncurable disease.

Zusammenfassung

Glioblastome (GBM) sind die häufigsten und aggressivsten primären Hirntumore bei Erwachsenen, mit einer Lebenserwartung von nur 12-15 Monaten ab der Diagnose und einer 5-Jahres-Überlebensrate von 5%. Trotz intensiver Forschung haben sich die Behandlungsergebnisse für GBM in den letzten Jahrzehnten kaum verbessert. Die Invasion von Tumorzellen in das umliegende Hirngewebe sowie die signifikante genetische und transkriptionelle Heterogenität erschweren Fortschritte in der Therapie.

In der hier vorgestellten Arbeit nutzen wir neuere Entwicklungen in der Generierung von Organoiden und der Einzelzellsequenzierung, um die Invasion von GBM-Zellen in Hirnorganoide experimentell zu modellieren. Wir etablieren humane Hirnorganoide basierend auf induzierten pluripotenten Stammzellen und kultivieren sie gemeinsam mit fluoreszenzmarkierten GBM-Zellen. Tumorzellen migrieren innerhalb von drei Tagen in die Organoide hinein und entwickeln membranumhüllte, schlauchförmige Ausstülpungen, genannt ‚microtubes', die bis zu 450 µm lang werden. Sie spiegeln damit die Ausbildung von Netzwerken aus Glioblastomzellen wider, die bereits *in vivo* beobachtet wurde. Mittels Gewebereinigung und Konfokalmikroskopie visualisieren und quantifizieren wir die Tumorinvasion. Unser Modell ist hochgradig skalierbar und reproduzierbar und ermöglicht so die Untersuchung des Invasionsprozesses innerhalb klinisch relevanter Zeiträume von weniger als einem Monat in Hochdurchsatzverfahren.

Einzelzell-Transkriptomanalysen von GBM-Zellen vor und nach Ko-Kultur mit Organoidzellen offenbaren erhebliche Heterogenität zwischen Patienten, identifizieren aber auch übereinstimmende transkriptionelle Veränderungen über alle Patienten hinweg, die generell zur Interaktion von Tumorzellen mit normalen Hirnzellen beitragen könnten. Neuartige Behandlungsstrategien, die auf die Tumorinvasion und die Bildung von ‚microtubes' abzielen, könnten daher zukünftig klinischen Nutzen für Patienten mit Glioblastomen bringen.

Insgesamt demonstrieren unsere Ergebnisse die Anwendung unseres experimentellen Systems zur Modellierung der Invasion von Glioblastomen *in vitro*. Unser Modell kann dazu beitragen, unser Verständnis dieser bislang unheilbaren Erkrankung zu verbessern, zielgerichtete Therapien zu entwickeln und personalisierte Behandlungsstrategien zu ermitteln.

1 Introduction

1.1 Invasive behaviour and cellular heterogeneity of glioblastoma

Glioblastoma (GBM) is the most frequent primary adult brain tumour, and also the most lethal (Omuro and DeAngelis, 2013; Ricard et al., 2012). In the WHO classification of gliomas, it is designated based on histopathological features as a grade IV tumour with a high rate of proliferation and aggressive invasion into the surrounding brain tissue. The current 5-year survival rate of GBM is estimated at 5%, and the expected survival time is only 12-15 months from diagnosis. These numbers have barely improved over the past decades, despite intensive research into GBM biology and novel therapies (Geraldo et al., 2019).

In the vast majority of cases, the origin of GBM remains unknown. Environmental exposure to ionising or electromagnetic radiation, viral infections, and genetic predisposition are all being investigated as potential causative factors, but their relevance has not been clearly established. A critical germline alteration predisposing patients to different tumour types including GBM has only been detected in a small minority of patients (<5%). Multigenetic predisposition also appears to play a minor role, since fewer than 20% of GBM patients present with a family history of malignancies (Wrensch et al., 2002).

As GBM tends to cause unspecific symptoms and diagnostic tools for early detection are not in routine clinical use, the cancer is typically diagnosed by standard magnetic resonance imaging at an advanced stage (Müller Bark et al., 2020). At this point, GBM presents with invasive projections that diffusely invade into the surrounding healthy brain tissue. Curative resection is therefore not feasible; instead, the therapeutic approach of choice is usually partial resection followed by adjuvant radiochemotherapy (Lara-Velazquez et al., 2021). Dissemination of GBM cells to distant locations also likely contributes to the high rate of recurrence observed for this entity (Paw et al., 2015).

Recent studies have demonstrated the striking invasive potential of GBM cells *in vivo* through histopathology and the use of mouse models. In post-mortem brain samples of GBM patients, widespread dissemination of tumour cells throughout both hemispheres and into the cerebrospinal fluid has been observed (Onda et al., 1989). A set of recent studies used multiphoton laser-scanning microscopy to track the dynamics of human GBM-derived cells injected into mouse brains for up to one year, finding that invasive GBM cells extend membrane-bound protrusions, termed microtubes, over distances of up to several hundred micrometres (Osswald et al., 2015). These protrusions enable GBM cells to interconnect over long distances and communicate via microtube-associated gap junctions. They also render the resulting GBM cell network more resistant to cell ablation, as tumour microtubes are used for cell replacement by advancing nuclei to the locations of dead cells within a few days. Finally, toxic levels of small molecules that occur in individual cells in response to chemotherapy or radiotherapy can be distributed via tumour microtubes across the larger network to result in nonlethal levels, making those therapies less effective (Weil et al., 2017). In addition to communicating with other tumour cells, GBM cells are also thought to interact with cells of the surrounding healthy brain tissue via soluble factors or direct cell-cell contacts, resulting in increased proliferation and invasiveness of the tumour (Broekman et al., 2018).

Apart from its invasive nature impeding complete surgical resection, another challenge in the treatment of glioblastoma is the substantial degree of cellular heterogeneity observed between and within tumours, which is becoming increasingly evident at the genetic (Meyer et al., 2015; Sottoriva et al., 2013), epigenetic (Klughammer

et al., 2018; Mazor et al., 2016) and transcriptional level (Patel et al., 2014). Based on integrated genomic and transcriptomic analyses of primary tumours, a classification comprising four transcriptional subtypes of GBM (termed Proneural, Neural, Classical and Mesenchymal) has been established (Verhaak et al., 2010). These subtypes may reflect different disease aetiologies or cells of origin of the tumours, and they have clinical relevance as different subtypes might be susceptible to different therapeutic approaches.

1.2 Modelling glioblastoma invasion *in vitro*

Due to the therapeutic and prognostic significance of the invasive behaviour of GBM, substantial effort has already been invested in understanding the underlying biological mechanisms and cellular dynamics. Attempts to study GBM invasion *in vivo* have largely been limited to mouse models, usually involving the injection or transplantation of human GBM cells into a living murine host. While such models may capture the systemic response to GBM progression, they are time-consuming and costly, with limited reproducibility, and they do not take into account the increased diversity of cell types in human compared to murine brains (Miller et al., 2019). Therefore, a recent study aimed to infer functional characteristics of individual invasive GBM cells *in vivo* from surgical biopsies of human patients, although results remained preliminary due to the low number of cells for which data could be obtained (Darmanis et al., 2017).

As an alternative approach to study GBM invasion, a variety of *in vitro* model systems have been developed in recent years that reproduce distinct characteristics of the disease. Most simply, GBM cells may be seeded onto artificial extracellular matrix materials, usually collagen-based, and their migration patterns tracked over time in three dimensions. However, these materials are an incomplete reproduction of the tumour microenvironment, remaining devoid of non-tumour cell types and often also lacking important components of the extracellular matrix such as laminin, proteoglycans and fibrous glycoproteins (Vollmann-Zwerenz et al., 2020).

To represent the cellular microenvironment of GBM more completely, organotypic slice cultures offer a model system preserving tissue architecture and three-dimensional (3D) structure *in vitro*. They have become a useful tool for investigating cellular processes in neuroscience as they are amenable to biochemical assays, immunohistochemical stainings, and microscopic imaging of fixed or living tissues (Humpel, 2015). Brain slice cultures are most often acquired from mice or rats, but to faithfully reproduce the cell type diversity of the human brain, they may also be obtained from human fetal tissue.

Based on recent advances in stem cell technologies, human organoids have emerged as an alternative system to model human tissues without the reliance on fetal samples. Brain organoids enable modelling of the healthy human brain as well as brain diseases *in vitro*. As they are usually derived from neural progenitor cells, human brain organoids recapitulate the development of neuronal and glial cells, while interactions with immune cells and other resident cell types may be modelled using co-culture protocols. Organoids have been used successfully to study the mechanisms underlying diverse neurodevelopmental and neurodegenerative diseases, as well as for drug screening applications (Chiaradia and Lancaster, 2020).

To model glioblastoma, recent studies have employed genetic transformation of human brain organoid cells into malignant cells, or transplantation of patient-derived tumour cells into organoids, to trace tumour progression *in vitro* (Bian et al., 2018; da Silva et al., 2018; Linkous et al., 2019; Ogawa et al., 2018). A major challenge of currently available organoid-based models for glioblastoma is the length of time required to establish and maintain

cultures, usually many weeks to months, limiting their usability for clinical applications. Moreover, the invasive behaviour of GBM cells and their interactions with healthy brain cells have not been studied in detail using these models. To achieve this, appropriate imaging technology is required for morphological assessments, while a comprehensive functional characterisation of individual tumour and non-tumour cells may be achieved by novel RNA sequencing approaches.

1.3 Imaging tumour invasion

Imaging the invasion of tumour cells into tissues by microscopy poses considerable technological challenges. As migrating GBM cells may traverse distances of more than 500 μm (Osswald et al., 2015), large tissue samples need to be imaged in order to track this process. Cryosectioning of samples, a method frequently chosen to visualise the architecture of many other solid tumours, enables the subsequent imaging of adjacent sections and reconstruction of a three-dimensional map of the locations of cell bodies or nuclei. However, the faithful tracing of tumour microtubes – which are of prime interest in the case of GBM – requires imaging of intact three-dimensional tissue samples. Different microscopy techniques have been developed over the past decades that can be used to address this challenge.

Confocal microscopy, an imaging technique which uses a spatial pinhole or confocal aperture to block any emission of light from out-of-focus planes, excites a specimen within a narrow plane of focus (Smith, 2011). Compared to conventional widefield fluorescence microscopy, this leads to a reduction in background signal. By moving the focus plane sequentially through the sample in a process known as optical sectioning, large three-dimensional objects can thus be imaged at superior optical resolution and contrast up to depths of several hundred micrometres. However, while detection of signal is limited to a single plane, confocal microscopy requires the illumination of the specimen with a double inverted cone of light, resulting in significant photobleaching and photodamage.

For samples that require penetration even deeper into the tissue, two-photon microscopy represents another promising technological advance (Kobat et al., 2011). While classic fluorescence microscopy relies on the excitation of a fluorophore by absorption of one single photon of a particular wavelength, two-photon microscopy uses the combined energy of two photons of a longer wavelength to excite a fluorophore. As the excitation volume is limited to the small part of the sample where two photons of appropriate energy are absorbed by the fluorophore almost simultaneously, no pinhole aperture is needed for this approach to reduce background signal. The longer wavelength photons used in two-photon microscopy are typically in the infrared region; they penetrate tissue more deeply and result in less tissue damage due to their lower energy levels, making two-photon microscopy particularly valuable for imaging live samples. The main drawback of this technology is the long acquisition time necessitated by pointwise scanning of the sample.

Light-sheet microscopes, on the other hand, enable high-resolution imaging of intact three-dimensional samples with fast acquisition speeds (Kumar et al., 2014; Power and Huisken, 2017; Wu et al., 2013). Here, illumination and detection axes are separated such that fluorophores are excited in a single thin layer with a scanning beam, and emitted light is detected along an orthogonal axis. This approach results in superior optical sectioning and improves the signal-to-noise ratio while also enabling fast acquisition speeds and low phototoxicity. However, the penetration depths offered by current commercially available light-sheet microscopes remain limited compared to two-photon microscopes.

Apart from choosing an appropriate imaging instrument, sample processing prior to imaging is another key determinant of image quality when visualising tumour invasion into tissues. A growing number of tissue clearing techniques have been developed that aim to reduce light scattering within the tissue during image acquisition by harmonising the refractive index throughout the sample. Broadly, current tissue clearing methods may be grouped into two categories: solvent-based techniques, which usually consist of tissue dehydration followed by lipid solvation and clearing through matching the refractive index to that of the dehydrated sample, and aqueous-based techniques, in which the sample is immersed in a solution with the same refractive index, sometimes following active or passive removal of lipids (Richardson and Lichtman, 2015). As different tissue clearing approaches have distinct advantages and drawbacks, for example with regard to changes in tissue architecture such as shrinkage or swelling, preservation of fluorescent protein emission or compatibility with immunolabelling protocols, a suitable approach needs to be selected for each individual application.

1.4 Single-cell transcriptomics

Solid tumours represent complex multicellular ecosystems, with diverse neoplastic cells surrounded by immune and stromal cell types. The rapid development of single-cell RNA sequencing (scRNA-seq) technologies during the past decade has enabled the study of functional cellular heterogeneity in human tumours at unprecedented resolution (Suvà and Tirosh, 2019).

While many different commercial and custom approaches now exist for analysing the transcriptomes of individual cells, they usually follow the same sequence of steps. Firstly, single cells are isolated from three-dimensional tissues by manual or enzymatic dissociation. RNA extracted from single cells is then reverse transcribed into cDNA libraries, which are subsequently amplified and sequenced using next-generation sequencing. Raw sequences are computationally aligned to the human genome, resulting in read counts per transcript for each cell. These read count distributions are finally subjected to downstream analysis, for example in order to determine cellular identities, resolve functional diversity, or infer potential interactions between cell types. As single-cell RNA sequencing data is inherently sparse and noisy, computational and statistical approaches have been developed that specifically deal with the analytical challenges imposed by this data (Stegle et al., 2015). For instance, methods that correct for technical variability and batch effects through adaptations of principal component analysis or the detection of mutual nearest neighbours now allow for the merging of transcriptomics data from different experiments (Butler et al., 2018; Haghverdi et al., 2018).

The first realisations of single-cell RNA sequencing relied on manual pipetting, but a number of commercial systems now simplify the processing of many individual cells in parallel through harnessing microfluidics or robotics. The WaferGen iCell8 system, which was used for the experiments presented in this thesis, dispenses a solution of single cells at limiting dilution into a chip containing 5,184 nanowells. An integrated microscope is employed to identify nanowells containing viable single cells, which are then processed for cDNA library generation. More recent commercial scRNA-seq technologies, such as the popular 10x Genomics Chromium system, can process several thousand cells at once and offer a more user-friendly setup with a smaller bench footprint.

For glioblastoma, scRNA-seq studies have already uncovered different malignant cell states and transcriptional programmes related to e.g. proliferation and immune signalling, with substantial heterogeneity between patients

(Neftel et al., 2019; Patel et al., 2014). However, GBM invasion and the interaction of tumour cells with normal human brain cells have not been specifically addressed yet.

1.5 Aims and significance of the current work

In the work presented here, we developed an experimental model system to study glioblastoma invasion into human brain organoids in a reproducible manner on clinically relevant timescales of less than one month. Our aim was to study the invasion process by imaging and single-cell transcriptome analyses. To this end, human brain organoids were generated from induced pluripotent stem cells (iPSCs) and co-cultured with fluorescently labelled patient-derived GBM cells. Invasion was visualised and quantified using confocal microscopy on previously cleared tissues. To study the interaction of GBM cells and normal brain cells of the neuronal lineage at a functional level, scRNA-seq was performed on tumour cells before and after co-culture with organoid cells. Our combined experimental and computational approach thus allowed us to identify transcriptional programmes implicated in GBM invasion and suggest potential therapeutic targets.

2 Methods and Materials

Sections in the following chapter are reproduced, with minor adaptations, from the corresponding publication (Krieger et al., 2020), and were written by myself. All experiments and analyses were performed by myself, unless otherwise indicated.

2.1 Glioblastoma cell culture

Primary tumour samples were received from Frankfurt University Hospital (Edinger Institute). Informed consent was obtained prior to surgery. Experiments involving human patient material were performed in accordance with the Declaration of Helsinki and were approved by the ethics committee of the University Cancer Center Frankfurt, project number SNO_01_13. Patient-derived GBM cell cultures were established by our collaborators Dr. Tanja Eisemann, Dr. Heike Peterziel and Prof. Peter Angel at the German Cancer Research Center, as described (Eisemann et al., 2019), and were transferred to our laboratory after cell dissociation and freezing. After thawing, we cultured cells in suspension culture in 75 cm^2 ultra-low attachment flasks in Neurobasal medium (Gibco) supplemented with 2 mM L-glutamine (Life Technologies), 1x B27 (Gibco), 2 µg/ml heparin, 20 ng/ml EGF and 20 ng/ml bFGF (R&D Systems). For passaging, spheroid cultures were dissociated using Accutase (StemCell Technologies) when they had reached diameters of ~100 µm, every 1-3 weeks. To confirm the invasive capacity of GBM cells in hydrogel matrix, spheroids were embedded in Matrigel (Corning).

2.2 Lentiviral labelling and FACS sorting

Second-generation replication-incompetent lentivirus was produced by FuGENE transfection (Promega) of HEK293T cells with the expression plasmid LeGO-G2, complemented with the packaging plasmids psPAX2 and pMD2.G (all from Addgene). GBM cells were infected on three consecutive days by spinoculation at 800 g for 30-60 minutes, and GFP-expressing cells were isolated by FACS. Lentivirally labelled GBM cells were maintained in neural maintenance medium, a 1:1 mixture of N-2 and B-27-containing media (N-2 medium: DMEM/F-12 GlutaMAX, 1× N-2, 5 µg/ml insulin, 1 mM L-glutamine, 100 µm nonessential amino acids, 100 µM 2-mercaptoethanol; B-27 medium: Neurobasal, 1× B-27, 200 mM L-glutamine), and passaged every 1-3 weeks as described above.

2.3 Cerebral organoid culture

The iPS cell line 409b2 was obtained from Riken Institute (Wako, Japan). For routine culture, iPSCs were maintained in mTeSR1 medium (StemCell Technologies) on tissue culture plates coated with Matrigel (Corning) and passaged every 4-5 days using Gentle Cell Dissociation Reagent (StemCell Technologies). For organoid seeding, iPSCs were dissociated with Accutase (StemCell Technologies) and transferred into AggreWell plates in Neural Induction Medium (StemCell Technologies) with 10 µM Y-27632 (StemCell Technologies) at a density of 1,000 cells per cavity, following manufacturers' instructions. Spheroid formation was confirmed visually after 24 hours, and spheroids were maintained in Neural Induction Medium (StemCell Technologies) with daily medium changes. After 5 days, spheroids were harvested from the AggreWell plates and embedded in Matrigel. Medium was changed to neural maintenance medium, supplemented with 50 U/ml penicillin and 50 mg/ml streptomycin, and exchanged every 2 days. Neural induction in 2D was performed after plating dissociated iPSCs onto Matrigel-coated plates, using the same culture media.

2.4 Glioblastoma invasion assays

2.4.1 Invasion into cerebral organoids

On day 24 of culture, organoids were removed from Matrigel by incubation with Dispase (Sigma) at 37°C, and transferred to individual wells of a GravityTRAP ULA Plate (PerkinElmer). Labelled GBM cells were dissociated with Accutase and added to the organoid plate in neural maintenance medium at a concentration of 1,000 cells per well. Plates were centrifuged at 100 g for 3 min before returning to the incubator. After 2 days, Organoids were live stained with 100 nM SiR-actin (Spirochrome). The following day, organoids were harvested, fixed in 2% PFA for 30 min, and embedded in Matrigel for immobilization.

2.4.2 Invasion into MCF10AT spheroids

MCF10AT cells were cultured in DMEM/F12 medium (Invitrogen) supplemented with 5% horse serum, 20 ng/ml EGF, 0.5 mg/ml hydrocortisone, 100 ng/ml cholera toxin, 100 µg/ml insulin and 1% penicillin/streptomycin. For organoid generation, single MCF10AT cells were plated in Matrigel (Corning) and allowed to develop for 14 days. MCF10AT spheroids were then dissociated with Dispase and co-cultured with dissociated GBM cells in neural maintenance medium in GravityTRAP ULA Plates, as described for cerebral organoid co-cultures.

2.4.3 Invasion into SH-SY5Y spheroids

SH-SY5Y cells were cultured in neural maintenance medium. To generate spheroids, cells were plated in a GravityTRAP ULA Plate (PerkinElmer) at a density of 5,000 cells per well and allowed to develop for 7 days. SH-SY5Y spheroids were then co-cultured with dissociated GBM cells in neural maintenance medium, as described for cerebral organoid co-cultures.

2.5 Tissue clearing of fixed organoids and spheroids

Adapting a previously published method (Hou et al., 2015), tissue clearing of Matrigel-embedded organoids was performed with an increasing gradient of fructose solutions over several days (Table 1).

Table 1: Composition of tissue clearing media
(adapted from Krieger et al., 2020)

Step	*Ingredients of clearing solution (wt/vol)*			*Duration of incubation*
	Fructose	*Urea*	*α-thioglycerol*	
1	35%	48% (8 M)	0.5%	12 hours
2	40%	48% (8 M)	0.5%	12 hours
3	60%	37% (6.16 M)	0.5%	24 hours
4	80%	26% (4.3 M)	0.5%	24 hours
5	100%	11% (1.8 M)	0.5%	24 hours
6	100%	11% (1.8 M)	0.5%	until imaging

2.6 Immunohistochemistry of organoid slices

For immunohistochemistry, organoids were fixed with 2% PFA for 30 min, embedded in Tissue-Tek O.C.T. compound, and snap-frozen in liquid nitrogen. Frozen samples were stored at -80°C for up to two weeks. Cryosections of 8 µm thickness were prepared by Dr. Anja Kühl at the Charité iPATH facility, and slides were stored at -20°C. Immunohistochemistry was performed with primary antibodies against KI67 (BD Bioscience

#610969), OCT4 (Abcam ab19857), βIII-tubulin (BioLegend #801202), PAX6 (BioLegend #901301), GPC3 (Sigma HPA006316), CD81 (Invitrogen MA5-13548), DLK1 (Invitrogen MA5-15915), NOTCH1 (CST 4380), COL4A5 (LSBio LS-C353940), ITGAV (Abcam ab16821), β-actin (Abcam ab8226), Cx43 (Sigma C6219), GFP (Abcam 13970), and appropriate secondary antibodies (Cell Signaling Technology).

2.7 Imaging

Confocal images were acquired on an LSM780 Axio Observer confocal laser scanning microscope (Zeiss).

2.8 Image analysis

2.8.1 Image pre-processing

Image pre-processing was performed in ImageJ as follows: To obtain a representation of the organoid, the SiR-actin signal was subjected to brightness adjustment and Gaussian blurring (sigma = 2), followed by scaling to 2912 μm^3/voxel by bicubic interpolation, and binarization using the Triangle method. To identify the voxels occupied by GBM cells, the GFP signal was subjected to brightness adjustment and Rolling-Ball background subtraction (radius = 64), followed by scaling to 2912 μm^3/voxel by bicubic interpolation, and binarization using Otsu's method.

2.8.2 Analysis of GBM invasion images

Downstream image processing was performed in MATLAB as follows: Using binarized images, single cells in the Matrigel surrounding organoids were excluded by connected component analysis using the 'bwlabeln' function, and holes inside the organoid were filled with the 'imfill' function. The organoid surface was approximated by Delauney triangulation using the 'delaunayTriangulation', and normal distances from GBM-occupied voxels to the organoid surface were calculated with the 'point2trimesh' function. We performed hierarchical clustering of voxels based on Euclidean distances and calculated distance matrices to visualize dispersion of GBM cells within organoids.

2.8.3 Tracing of microtube processes

Processes were tracked using the Simple Neurite Tracer in ImageJ. A total of 120 cells (n=10 cells each from n=3 organoids for each patient) were randomly selected, and all their processes tracked.

2.9 Single-cell RNA sequencing

2.9.1 Isolation of single cells

For scRNA-seq of GBM cell lines, cells were cultured in neural maintenance medium for 1-3 weeks after passaging, until the largest spheroids were ~100 μm in diameter. Cells were then dissociated with Accutase (StemCell Technologies), washed twice in PBS, and passed through a 20μm cell strainer (PluriSelect).

For scRNA-seq of co-cultured GBM and organoid cells, NPC spheroids were generated by inducing iPSCs AggreWell plates as described above. After 7 days, NPC spheroids and lentivirally labelled GBM cells from separate cultures were dissociated using Accutase (StemCell Technologies), mixed in a 1:1 ratio, and replated onto AggreWell plates at 1,000 cells per cavity in neural maintenance medium. After 3 days, mixed spheroids were dissociated using Accutase (StemCell Technologies), washed twice in PBS, and passed through a 20 μm cell strainer (PluriSelect).

2.9.2 Preparation of libraries for scRNA-seq

Single-cell suspensions were stained with Hoechst and Propidium Iodide (ReadyProbe Cell Viability Imaging Kit, Invitrogen) for 10 min at room temperature and cell numbers and viability were checked with a Countess automated cell counter (Thermo Fisher). Samples were discarded if cell viability was below 85%. The TakaraBio iCELL8 system and the associated Rapid Development Protocol (in-chip RT-PCR amplification) were used for single cell isolation, reverse transcription and cDNA amplification (Goldstein et al., 2017). Briefly, cell suspensions were distributed into a nanowell chip containing oligo-dT primers with a unique barcode for every well. Chips were imaged using an automated fluorescence microscope and frozen at -80°C until further use. Nanowells occupied by single cells were identified using the CellSelect software and manually curated in order to exclude non-detected doublets or dead cells. After thawing frozen chips, 50 nl of RT/Amp solution was dispensed into selected nanowells (Master mix: 56 µl 5 M Betaine, 24 µl 25 mM dNTP mix (TakaraBio), 3.2 µl 1 M $MgCl_2$ (Invitrogen), 8.8 µl 100 mM Dithiothreitol (TakaraBio), 61.9 µl 5x SMARTScribe™ first-strand buffer, 33.3 µl 2x SeqAmp™ PCR buffer, 4.0 µl 100 µM RT E5 Oligo, 8.8 µl 10 µM Amp primer (all TakaraBio), 1.6 µl 100% Triton X-100 (Acros), 28.8 µl SMARTScribe™ Reverse Transcriptase, 9.6 µl SeqAmp™ DNA Polymerase (TakaraBio)). After in-chip RT/Amp amplification (18 amplification cycles, in-chip RT/Amp Rapid Development protocol) inside a modified SmartChip Cycler (Bio-Rad), libraries were pooled, concentrated (DNA Clean and Concentrator−5 kit, Zymo Research) and purified using 0.6x Ampure XP beads. Concentration and quality of cDNA was assessed by a fluorometer (Qubit) and by electrophoresis (Agilent Bioanalyzer high sensitivity DNA chips). Next generation sequencing libraries were constructed using the Nextera XT kit (Illumina) following the manufacturer´s instructions. Final libraries were sequenced with the NextSeq 500 system in high-output mode (paired-end, 21 x 70 for v1, 24 x 67 for v2 chip). Raw sequencing data have been deposited at the European Genome-Phenome Archive (http://www.ebi.ac.uk/ega/) under accession number EGAS00001003852.

2.9.3 scRNA-seq data analysis

2.9.3.1 Pre-processing

For pre-processing of single-cell RNA-seq data, the following steps were performed by our collaborator Dr. Jeongbin Park, using an automated in-house workflow based on Roddy (https://github.com/TheRoddyWMS/Roddy). Read quality was evaluated using FastQC. iCELL8 library barcodes from the first 21 bp reads were assigned to the associated nanowell with the Je demultiplexing suite (Girardot et al., 2016). Remaining primer sequences, Poly-A/T tails and low-quality ends (<25) were trimmed using Cutadapt. Furthermore, since NextSeq (Illumina) encodes undetected bases as incorrect ‘Gs’ with high quality, Cutadapt’s ‘—nextseq-trim’ option was used for improved quality trimming. Trimmed reads were mapped to the reference genome hs37d5 (derived from the 1000 genomes project) using the STAR aligner. Mapped BAM files were quantified using featureCounts with reference annotation gencode v19.

2.9.3.2 Quality control and normalization

To exclude low-quality cells from further analysis, RNA-seq libraries that contained less than 150 detected genes or more than 15% mitochondrial reads were filtered out. Adapting a previously published approach (Puram et al., 2017), aggregate expression for each gene across all cells was calculated as $E_a = \log(\text{mean}[E_{j,1\ldots n}] + 1)$, where E_j is the counts-per-million expression value of the gene in cell j. 8,533 genes with $E_a > 2$ were retained for analysis.

2.9.3.3 Comparison of tumour cells from individual and co-cultured samples

Filtered and normalized data of all patients was combined to identify NPCs and tumour cells in each sample. Using the Seurat package as implemented in R (Butler et al., 2018), principal component analysis (PCA) was performed prior to clustering, and the 'FindClusters' function (with resolution = 0.4) was run on the first 9 principal components only. Results were visualized by t-distributed stochastic neighbour embedding (t-SNE (van der Maaten and Hinton, 2008)). Clusters containing cells from the NPC-only sample were identified as 'brain', whereas clusters containing only GBM cells were identified as 'tumour'. After manual splitting of one of the resulting clusters, we obtained 10 clusters representing brain cells (3 clusters), tumour cells from co-cultured samples, or tumour cells from unmixed samples.

Differential expression between mixed and unmixed tumour cells was evaluated using the 'FindMarkers' function in Seurat. Gene set enrichment analysis (Subramanian et al., 2005) was performed by computing overlaps between identified gene signatures and Gene Ontology (GO_C5) gene sets derived from the Molecular Signature Database (MSigDB, https://software.broadinstitute.org/gsea/msigdb). Cell state signature genes for G1/S and G2/M cell cycle phases were downloaded from a recent study (Neftel et al., 2019). Following their approach, cell state scores and cell cycle scores were computed using the 'AddModuleScore' function in Seurat. Cell cycle scores were calculated based on the combined list of G1/S and G2/M genes.

2.9.3.4 Analysis of ligand-receptor interactions

Potential receptor–ligand pairings were analyzed using 2,557 previously published receptor–ligand pairs consisting of 1,398 unique genes (Ramilowski et al., 2015), of which 317 were expressed in our data. Adapting a previously published approach (Camp et al., 2017), we constructed a cell-cell interaction matrix by summing for each pair of cells from the same sample the number of ligand-receptor pairs potentially connecting the pair, with one cell type expressing the receptor and the other the ligand (normalized expression cutoff > 0.5). To identify ligand-receptor interactions with likely significance for the invasion process, we then considered each ligand-receptor pair in turn, and calculated the number of cell pairs connected by this ligand-receptor interaction for each possible cell type combination (tumour–tumour, brain–brain, tumour–brain), for each sample. The resulting interaction matrix was normalized to the maximum possible number of cell-cell interactions. To identify ligand-receptor pairs with coherent differential expression across patients, we considered only those ligand-receptor pairs with mean normalized expression greater than 0.5 times the mean across all pairs for all tumour-only samples, all pairings from mixed samples where tumour cells express the ligand, all interactions from mixed samples where tumour cells express the receptor, or the NPC-only sample. These interactions were clustered based on complete linkage of Euclidean distances and visualized using the heatmap.2 package in R. For Gene Ontology (GO) analysis, we considered those ligand-receptor pairs with mean normalized expression greater than 0.5 times the mean across all pairs for one cell type interaction (GBM→NPC, NPC→GBM, GBM→GBM, NPC→NPC), and less than 0.5 times the mean for the other three. No putative GBM→GBM interactions fulfilled these criteria.

3 Results

Sections in the following chapter are adapted, with minor changes, from the corresponding publication (Krieger et al., 2020), and were written by myself. All experiments and analyses were performed by myself, unless otherwise indicated.

3.1 iPSC-derived cerebral organoids provide a scaffold for glioblastoma invasion

To study glioblastoma invasion in a physiologically relevant 3D context, we adapted an established protocol for human iPSC-derived cerebral organoid development (Lancaster and Knoblich, 2014) to achieve streamlined and reproducible production of organoids (Fig. 1A).

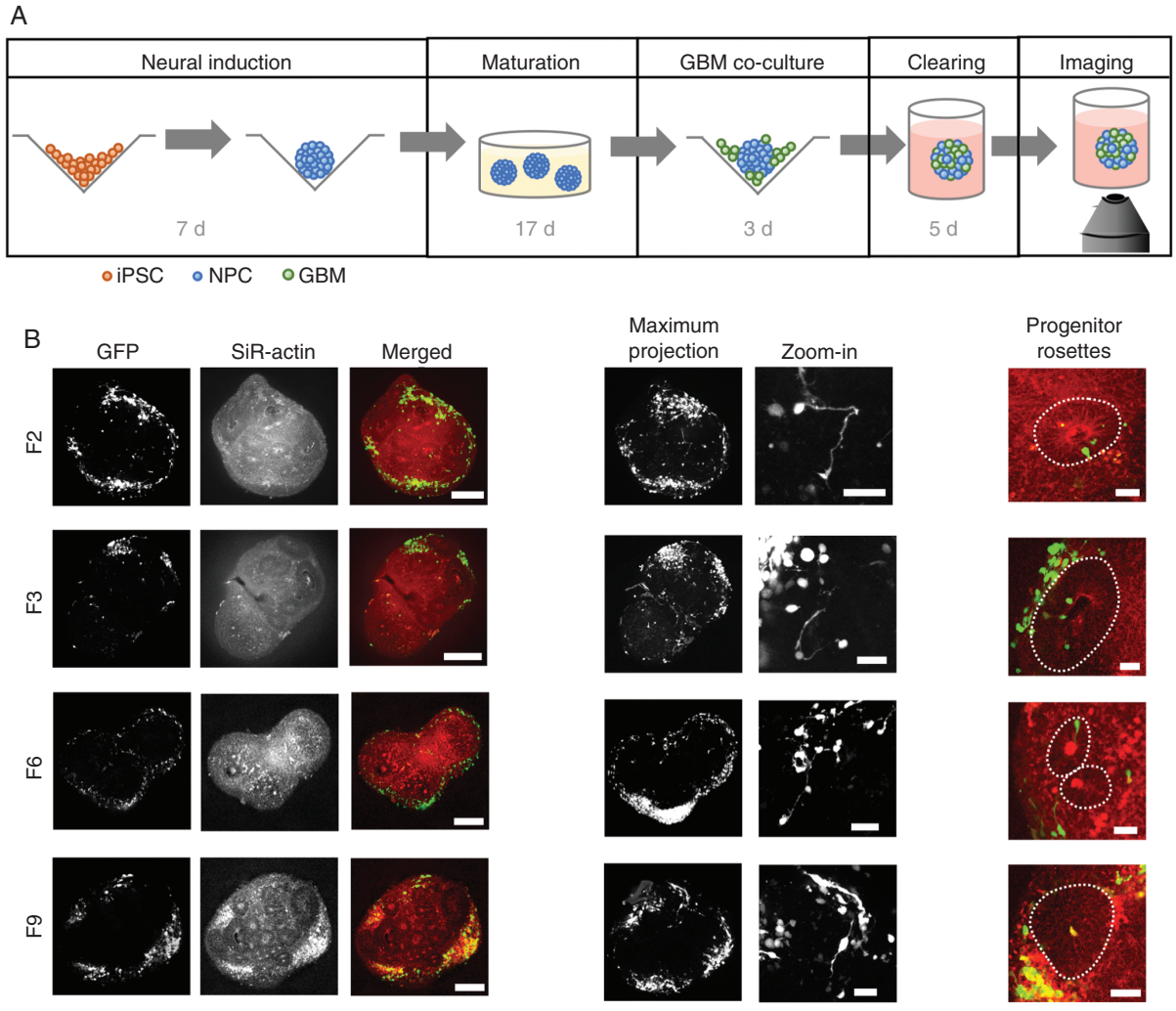

Figure 1: GBM invasion assay (A) Experimental protocol. Following 7 days of neural induction, organoids were transferred to Matrigel and matured for 17 days. Organoids were then enzymatically released and co-cultured with GFP-labeled GBM cells for 3 days. Samples were embedded in Matrigel again for fixation, tissue clearing and confocal imaging. (B) GFP-labeled tumour cells from all 4 GBM patients invade into cerebral organoids (left; scale bars, 250 µm) where they form short-range and long-range connections (middle, maximum intensity projections over ~200–250 µm depth; scale bars, 50 µm). Invasion is largely restricted to neuronal layers, outside of neural progenitor rosettes indicated by dotted lines (right; scale bars, 50 µm). (from Krieger et al., 2020)

From 24 days of age, cerebral organoids were co-cultured with fluorescently labelled glioblastoma cells from four patient-derived cell lines (Table 2). Samples were fixed after three days and subjected to tissue clearing using a fructose-based clearing protocol (Hou et al., 2015), enabling the visualization of tumour invasion by confocal microscopy. We found that tumour cells from all four GBM patients readily attached to and invaded into the organoids. Tumour cells formed protrusions reaching to other cells over short and long distances (Fig. 1B), consistent with tumour microtube formation observed *in vivo* in mice (Osswald et al., 2015). GBM cells primarily invaded into the neuronal layers of the organoids, with little invasion into neural progenitor rosettes. Conversely, we did not observe invasion of GBM cells into organoids grown from the breast cancer cell line MCF10AT or the neuroblastoma cell line SH-SY5Y.

Table 2: Cell line characteristics
(adapted from Krieger et al., 2020)

Cell line	Classification	Primary/ Recurrence	Sex	Age	Localization	Treatment	IDH^{-} (1)	ATRX^{+} (2)	MGMT promoter methylation
GBM-F2	Glioblastoma, WHO grade IV	Primary tumour	M	65	left occipital	none	✓	✓	✓
GBM-F3	Glioblastoma, WHO grade IV	Recurrence (after resection and re-resection)	M	52	right occipital	Radio-chemotherapy and surgery	✓	✓	unknown
GBM-F6	Glioblastoma, WHO grade IV	Primary tumour	M	68	right temporo-parietal	none	✓	✓	✓
GBM-F9	Glioblastoma, WHO grade IV (giant cell component)	Primary tumour	F	71	right temporal	none	✓	✓	✓
(1) No expression of IDH1_R132H detected. (2) Expression of ATRX detected.									

3.2 Tumour microtube formation recapitulates *in vivo* behaviour of GBM cells

We developed a semi-automated image processing workflow to analyse the invasion process quantitatively (Fig. 2A), which we applied to a total of 66 organoids (n=15-19 for each of the four patient GBM cell lines). We found that, for organoids of comparable sizes, the fraction of organoid volume taken up by tumour cells was similar across the four patient-derived cell lines (Fig. 2B). The distribution of glioblastoma cells within organoids was assessed by calculating the distances between GFP^{+} voxels across the same set of organoids. Tumour cells spread widely in all cases. To quantify invasion depth, we compared the distribution of distances of GFP^{+} voxels from the organoid surface across 12 similarly sized organoids for each patient-derived cell line. Invasion depths exceeded 100 µm in the majority of organoids (Fig. 2C), with some cells detected at approximately 300 µm from the organoid surface. While migration depth of the most invasive cells (90th percentile of invasion depth) was uncorrelated with organoid size, we observed that cells from patients F6 and F9 were less invasive than cells from patients F2 and F3 (Fig. 2D); this suggests that the *in vitro* model may be able to reproduce intertumour heterogeneity in invasive behaviour, although we cannot currently rule out that the observed differences in invasion depth stem from differences in 3D architecture between the scaffold organoids.

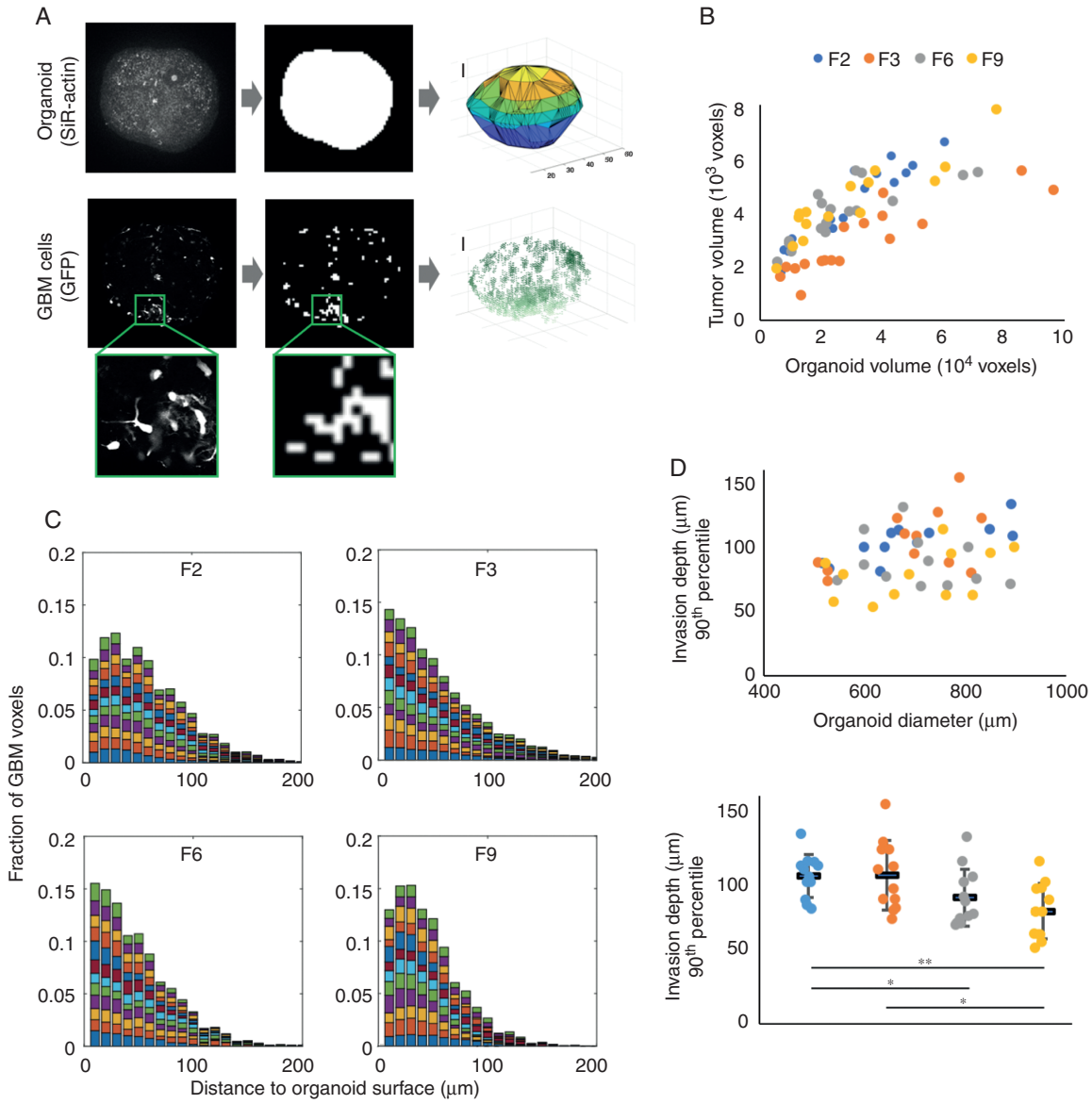

Figure 2: Morphological features of patient-derived GBM cells invading organoids (A) Image analysis workflow. To approximate the organoid surface, organoids were incubated with the live dye SiR-actin; following fixation and clearing, the actin signal was binarized and triangulated (top). Above-threshold GFP signal was used as a proxy for GBM cell location (bottom). Scale bars, 100 µm. (B) Total tumour cell volume as a function of organoid volume. (C) Distributions of distances of tumour voxels from the organoid surface of 12 organoids from each patient cell line with 500–900 µm diameter; each color represents one organoid. (D) Invasion depth of the most invasive cells from each cell line (90th percentile) compared with organoid size (top) and differences in invasion depth between patient cell lines (bottom; $*P < 0.05$, $**P < 0.01$, two-sided Student's *t*-test). In (D), black horizontal bars indicate mean values and error bars represent standard errors in the mean. (adapted from Krieger et al., 2020)

By tracing membrane-bound cellular processes in images, we found that the number of microtubes per GBM cell ranged up to 6, with 2.2±0.1 microtubes on average (Fig. 3A). We quantified how many of these microtubes ended at other GBM cells, and identified between 0 and 4 such putative intratumoural connections per GBM cell, with an average of 1.2±0.1 connections (Fig. 3B). Individual microtubes were up to 450 µm long (Fig. 3C). Consistent with our earlier observation of intertumoural heterogeneity of invasive capacity, we found that microtube lengths differed between cell lines (Fig. 3C). Interestingly, the cell lines with higher invasive capacity (F2 and F3) also

showed longer microtubes; this observation suggests that GBM tumours extending longer microtubes may be able to colonise organoids more efficiently *in vitro*, consistent with recent *in vivo* reports that microtubes promote tumour dissemination by allowing GBM cells to exchange cytoplasmic molecules and even translocate nuclei over long distances (Osswald et al., 2015; Winkler and Wick, 2018).

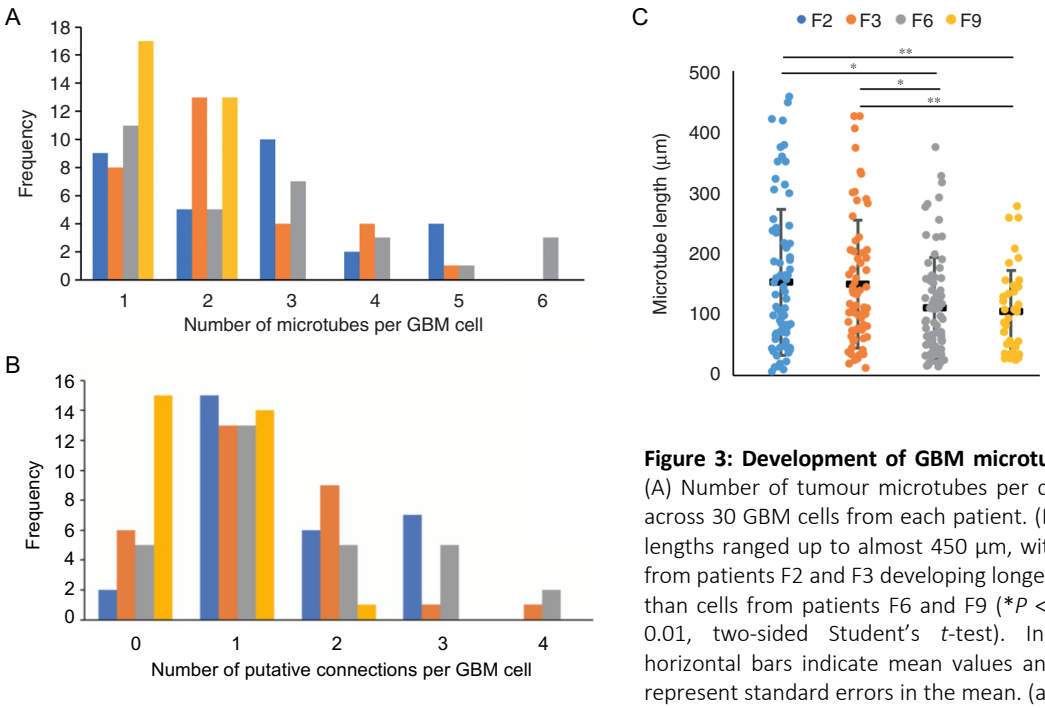

Figure 3: Development of GBM microtubes *in vitro* (A) Number of tumour microtubes per cell observed across 30 GBM cells from each patient. (F) Microtube lengths ranged up to almost 450 µm, with GBM cells from patients F2 and F3 developing longer microtubes than cells from patients F6 and F9 (*$P < 0.05$, **$P < 0.01$, two-sided Student's *t*-test). In (C), black horizontal bars indicate mean values and error bars represent standard errors in the mean. (adapted from Krieger et al., 2020)

3.3 scRNA-seq reveals transcriptional heterogeneity between tumours

Our imaging results confirm that iPSC-derived cerebral organoids represent an effective model system for quantifying GBM invasion and tumour microtube formation *in vitro*. To further study heterogeneity of and interactions between GBM and organoid cells at the transcriptome level, we developed a more efficient workflow that could be applied on clinically relevant timescales and at higher throughput. In the modified assay, dissociated 7-day-old cerebral organoids were mixed with GBM cells from separate cultures at a 1:1 ratio, and grown in co-culture for 3 days (Fig. 4A). GBM cells from all four patient-derived cell lines readily mixed with dissociated organoid cells (Fig. 4B). With or without addition of GBM cells, dissociated organoid cells efficiently re-established the characteristic architecture of progenitor rosettes and neuronal layers observed in cerebral organoids, and membrane protrusions emanating from tumour cells were visible in all samples (Fig. 4C). After 3 days of co-culture, mixed spheroids were dissociated and subjected to scRNA-seq. For comparison, we also dissociated and sequenced recomposed spheroids of organoid cells that had not been mixed with GBM cells, referred to as neural progenitor cells (NPCs) below, and GBM cells from all four patient-derived cell lines that had been grown separately as spheroids in the same culture medium (Fig. 4A).

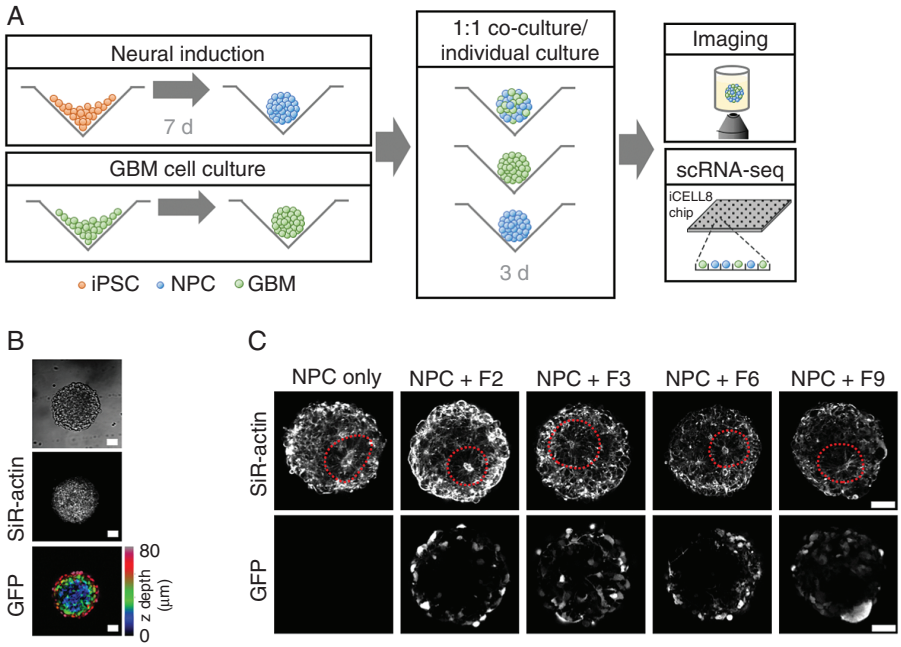

Figure 4: Co-culture assay of patient-derived GBM and organoid cells (A) Experimental protocol. Following 7 days of neural induction, organoids and spheroids of lentivirally labeled GBM cells grown separately were enzymatically dissociated and mixed at a 1:1 ratio. After 3 days of co-culture, mixed spheroids were subjected to imaging or scRNA-seq using the iCell8 system. (B) Tumour cells mixed efficiently with organoid cells. (C) With or without addition of GBM cells, dissociated organoid cells re-established the characteristic 3D architecture of neural rosettes within 3 days. Scale bars, 50 µm. (adapted from Krieger et al., 2020)

Following pre-processing and quality control, we obtained 5,083 single-cell transcriptional profiles with approximately 1,400 genes detected per cell on average (Fig. 5A). PCA-based clustering and 2D visualization by t-SNE maps revealed that GBM cells cultured alone clustered separately for each patient (clusters 5, 6, 7 and 9), confirming intertumoural heterogeneity (Fig. 5B). We further identified three clusters (clusters 0, 1 and 3) containing cells from the unmixed organoids as well as cells from all four mixed samples, and concluded that the latter represent the organoid cells in the mixed samples. The remaining clusters (clusters 2, 4 and 8) contain GBM cells from patients F2, F3 and F9 after co-culture with organoid cells. As only six such cells were identified in the mixed sample from patient F6, they were excluded from further analyses and not displayed here.

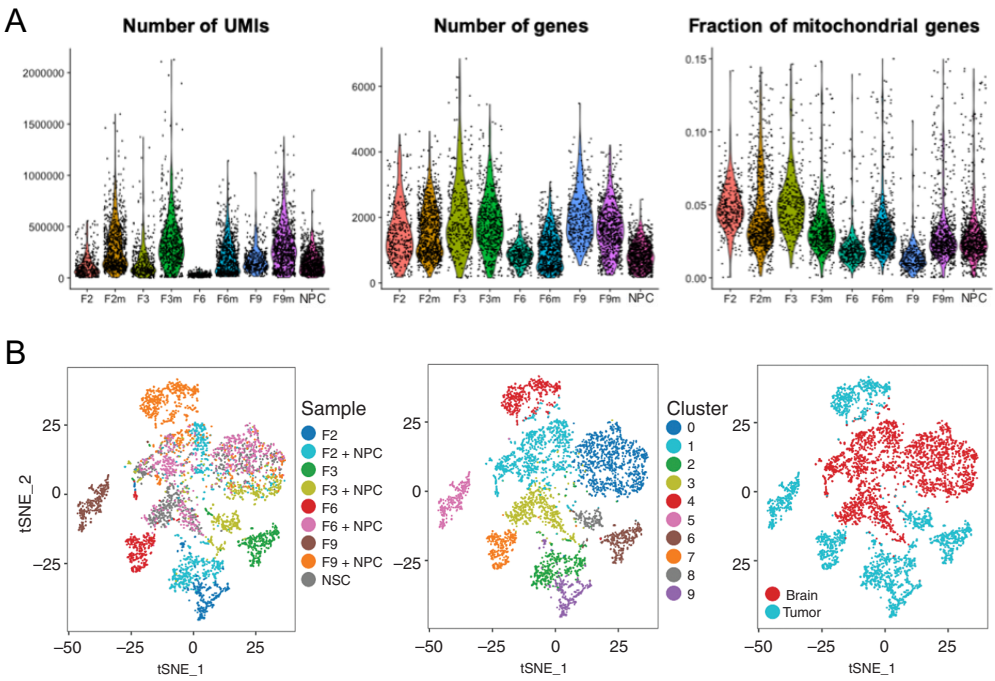

Figure 5: Single-cell transcriptome data from GBM co-cultured with organoid cells (A) The number of Unique Molecular Identifiers (UMIs), the number of genes, and the percentage of mitochondrial genes detected in each sample. F2 to F9: GBM cell lines, NPC: neural progenitor cells, m: co-cultures. (B) t-SNE map showing all cells after quality control and PCA-based clustering, coloured by sample origin (left), by cluster (middle), and by organoid or tumour cell identity (right). In addition to three clusters containing organoid cells, GBM cells clustered separately for each patient and before or after co-culture with organoid cells. (adapted from Krieger et al., 2020)

In agreement with previous scRNA-seq studies of GBM (Neftel et al., 2019; Patel et al., 2014), we detected heterogeneous expression of gene signatures defining the classical, mesenchymal, neural and proneural GBM subtypes (Verhaak et al., 2010) within each patient-derived cell line, indicating that they comprise cells most representative of more than one subtype (Fig. 6). On average, cells from patients F2 and F3 mostly corresponded to the mesenchymal subtype, while cells from patients F6 and F9 most closely matched the neural subtype; as the mesenchymal subtype has been characterized as the most invasive (Carro et al., 2010; Verhaak et al., 2010), this is consistent with our earlier observation that F2 and F3 display higher invasive capacity *in vitro*.

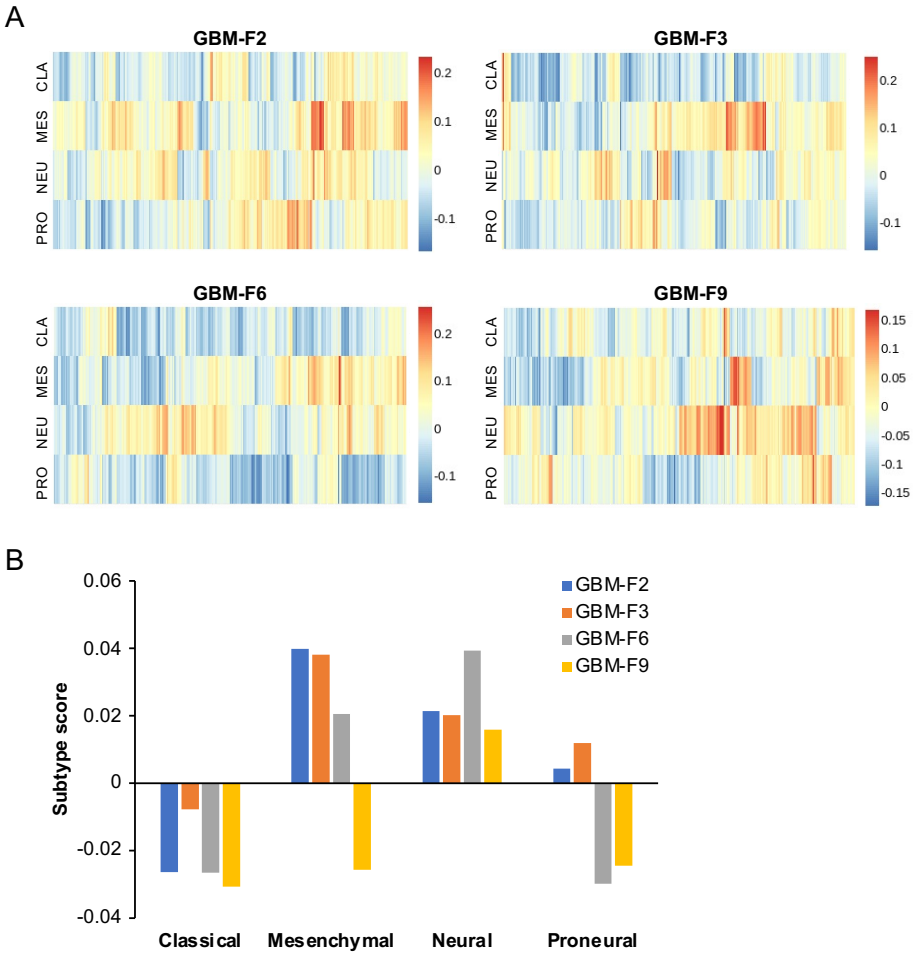

Figure 6: GBM subtype analysis of patient-derived cell lines (A) Subtype scores for the classical (CLA), mesenchymal (MES), neural (NEU) and proneural (PRO) GBM subtypes were computed for each cell based on the expression of 210 subtype signature genes (Verhaak et al., 2010), relative to the aggregated expression of control gene sets expressed at similar levels (Methods). (B) Average subtype scores for each patient-derived GBM cell line. (adapted from Krieger et al., 2020)

3.4 Mixing GBM and organoid cells leads to up-regulation of a shared set of genes across patients

Differential gene expression testing between GBM cell clusters from mixed and unmixed samples revealed hundreds of genes that were significantly up- or downregulated upon co-culture with organoid cells (adjusted p-value < 0.05, log(fold change) > 0.15), and an overlap of 45 genes that were upregulated in all patients (Fig. 7A). These included the homeobox transcription factor PAX6, normally expressed in forebrain neural stem cells; the gap junction protein alpha 1 (GJA1) coding for connexin-43, which connects tumour microtubes in GBM (Osswald et al., 2015); glypican-3 (GPC3), a cell surface heparan sulfate proteoglycan and Wnt activator whose expression correlates with invasiveness of hepatocellular carcinoma (Cheng et al., 2008); collagen COL4A5, an extracellular matrix constituent; and several lysosomal, vesicular and secretory proteins (Fig. 7B and Table 3). Gene set enrichment analysis of the 45 coherently upregulated genes confirmed that genes relating to growth regulation, neuronal migration, extracellular secretion and stimulus response were enriched in this group (Fig. 7C). Our results thus show that interactions between GBM and organoid cells increase expression of genes required for GBM

network formation and invasion, indicating that GBM cells sense the presence of neuronal cells and reactively amplify the transcription of genes supporting their dispersion.

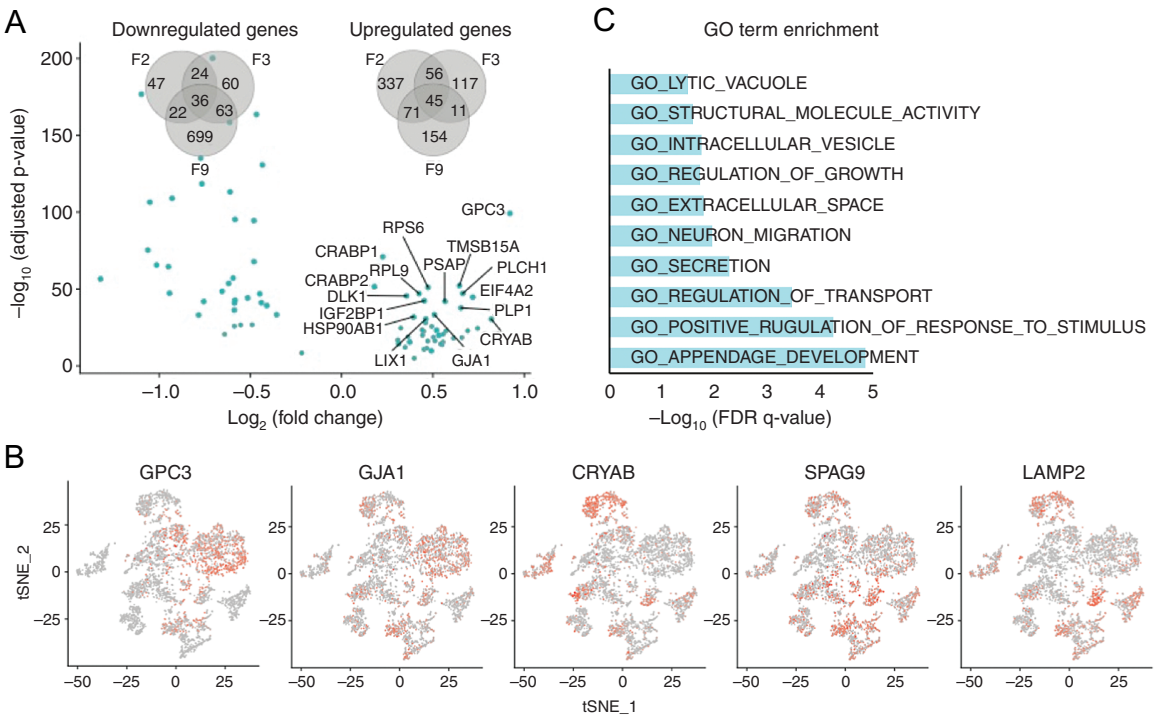

Figure 7: Single-cell RNA-seq analysis of GBM cell interactions with cerebral organoid cells (A) Volcano plot shows the 45 genes significantly up- or downregulated across all three patient-derived GBM cell lines upon co-culture with organoid cells (adjusted $P < 0.05$ for each patient separately). Venn diagrams quantify the overlap of differentially regulated genes detected from each patient. (B) Expression of differentially regulated genes visualized on a t-SNE map of all cells (t-SNE representation identical to Fig. 5B). (C) Gene Ontology–based gene set enrichment analysis of genes upregulated in all patient tumour cell lines upon co-culture with organoid cells. (adapted from Krieger et al., 2020)

Table 3: Genes coherently upregulated in GBM cell lines upon co-culture with organoid cells
(adapted from Krieger et al., 2020)

GPC3	ARGLU1	IGF2BP1	SPAG9	PRTG	EIF2S3	COPA	GNPDA1	COL4A5
CRABP1	TMOD3	ARRDC3	DLK1	HSPA8	POLA1	LARS	HSP90AA1	LAMP2
CRABP2	RPS6	SCG5	LIX1	POLR2B	PUM1	VPS41	CRYAB	KDM4A
PLP1	EIF4A2	PSAP	ANKRD36	ANKRD36C	NKTR	PAX6	BLOC1S5	COL4A5
PLCH1	RPL9	TMSB15A	SUGP2	MORF4L2	VPS13B	HSP90AB1	GJA1	LAMP2

3.5 Potential ligand-receptor interactions between tumour cells and organoid cells

To investigate the nature of interactions between GBM and organoid cells, we considered the expression of 2,557 known ligand-receptor pairs (Ramilowski et al., 2015) across our samples, comprising a total of 1,398 unique genes. Of these, 317 genes were expressed in our data, with approximately 13% expressed differentially between

the same cell types in unmixed and mixed samples (Fig. 8A). Calculating the number of potential interactions between brain and tumour cells based on the expression of complementary receptors and ligands, we detected substantial crosstalk between cell types (Fig. 8B). Hierarchical clustering of the number of cells potentially linked by each ligand-receptor pair revealed a group of ligand-receptor pairs that were expressed at low levels in the tumour-only and NPC-only cultures, but presented many potential interactions between tumour cells and organoid cells in the mixed cultures (Fig. 8C). These included several collagen-integrin interactions, glypican-3 binding to insulin-like growth factor 1 receptor (IGF1R) or the cell cycle regulator CD81, and non-canonical Notch signaling (DLK1/NOTCH1, DLK1/NOTCH2). Notably, despite the transcriptional heterogeneity we observed between patients, our approach detected consistently expressed potential interactions across all patient cell lines (Fig. 8C). Gene set enrichment analysis showed that the ligand-receptor pairs expressed at high levels in co-cultured samples are enriched for invasion-related genes (Fig. 8D). Specifically, putative interactions in which GBM cells present the ligand and NPCs the receptor are enriched for genes involved in neuron projection development and receptor binding, whereas ligand-receptor pairs communicating in the opposite direction are enriched for extracellular matrix proteins.

Many of the candidate ligand-receptor pairs identified in our analysis have been linked with glioblastoma progression by previous work. Glutathione S-transferase P (GSTP1) has been shown to bind tumour necrosis factor receptor-associated factor 2 (TRAF2) *in vivo* and *in vitro*, attenuating tumour necrosis factor (TNF) signaling and thus enhancing resilience in tumour cells[34]. Notch receptors 1 and 2 are known to associate with the transmembrane protein Delta Like Non- Canonical Notch Ligand 1 (DLK1), but downstream effects in glioblastoma remain unclear and may depend on heterogeneous cell states within the tumour[35]. Binding of collagens to integrins, integrin-associated protein CD47 or Discoidin Domain Receptor Tyrosine Kinase 1 (DDR1) all correlate with glioblastoma proliferation and invasion[36–39]. Integrin α6 (ITGA6) as a receptor for the extracellular matrix protein laminin (LAMA1) has also been detected in patient specimens of glioblastoma and contributes to cancer stem cell proliferation *in vitro*[40].

In addition to confirming these established signalling interactions, our *in silico* screen suggests putative interactions which may provide novel therapeutic targets for glioblastoma. Our results suggest Adherens Junction Formation Factor (AFDN/MLLT4) as a ligand activating EPH Receptor A7 (EPHA7), which has been linked to adverse outcome in primary and recurrent glioblastoma[44]. Moreover, binding of GPC3 to IGF1R or CD81 is known to contribute to hepatocellular carcinoma development and invasiveness[41]; immunotherapies targeting GPC3, which are showing promise in hepatocellular carcinoma[42,43], may also benefit glioblastoma patients.

To validate our findings, we performed immunohistochemistry on cryosections of co-culture spheroids comprising NPCs and GBM cells to detect putative ligand-receptor interactions revealed by scRNA-seq. As predicted, we observed ligand-receptor pair expression of non-canonical Notch signalling proteins (DLK1/NOTCH1), GPC3/CD81, and COL4A5/ITGAV (Fig. 9A), in GBM cells and NPCs within co-culture spheroids. Moreover, expression of NICD1 (the cleaved intracellular domain of NOTCH1), indicating NOTCH1 activation, tended to increase in GBM cells in co-cultures compared to monocultures (Fig. 9B). These results indicate that GBM and organoid cells within co-cultures interact via the expression of receptors and their respective ligands.

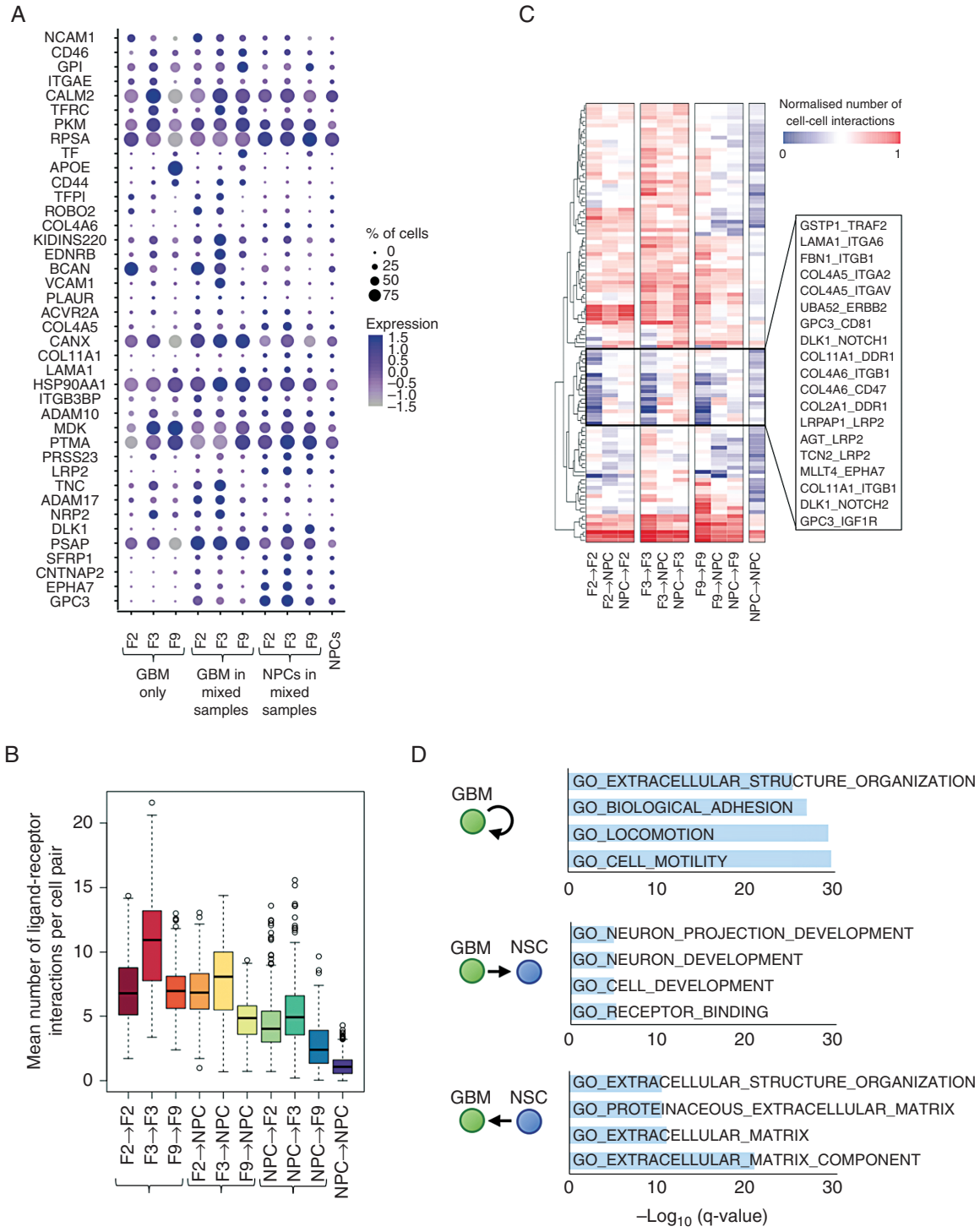

Figure 8: Potential ligand–receptor interactions between GBM and organoid cells (A) Expression of ligand and receptor genes that are significantly upregulated in NPCs or in at least one GBM cell line upon co-culture (adjusted $P < 0.05$), averaged across GBM-only samples (left), GBM cells, or NPCs within mixed samples (middle), and the NPCs-only sample (right). Dot size corresponds to the fraction of cells expressing the gene in each group; dot color represents the average expression level. (B) The mean number of ligand–receptor pairs potentially connecting cells pairs of the given cell types, based on RNA expression levels across GBM-only samples (left), GBM cells, or NPCs within mixed samples (middle), and the NPCs-only sample (right). Center line, median; box limits, upper and lower quartiles; whiskers, 1.5x interquartile range; points, outliers. (C) Mean number of cell-cell interactions for different cell type combinations and selected ligand–receptor pairs. Hierarchical clustering reveals a group of ligand–receptor pairs (middle box) that are expressed at low levels in GBM cells or NPCs alone, but are upregulated upon co-culture. (D) Gene Ontology–based gene set enrichment analysis of ligand–receptor pairs preferentially expressed in the given cell type combinations. (adapted from Krieger et al., 2020)

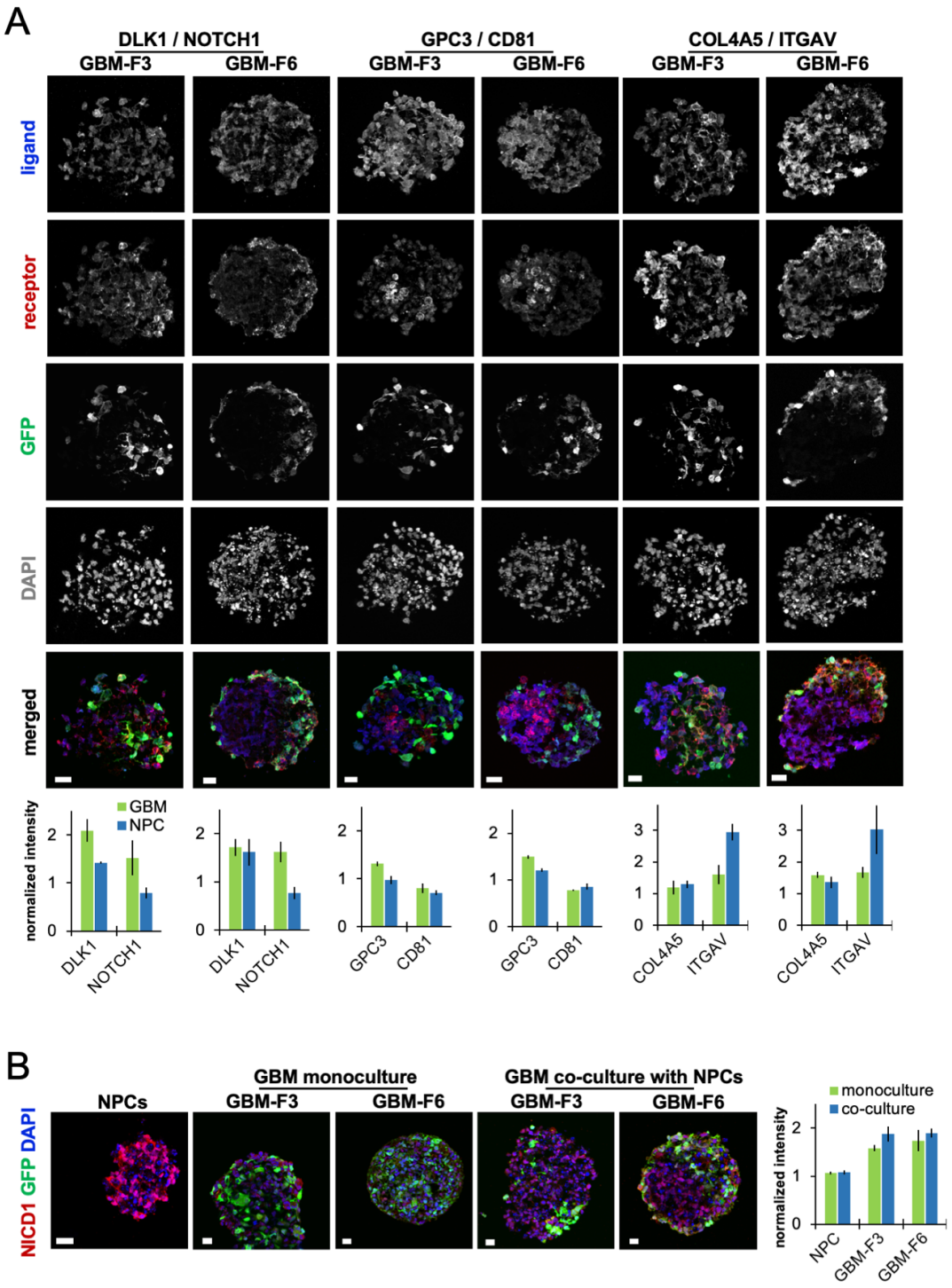

Figure 9: Changes in GBM ligand-receptor pair expression upon co-culture (A) Immunohistochemistry images show expression of ligand-receptor pairs in cryosections of co-culture spheroids comprising NPCs and GBM cells from patients F3 or F6. The bottom images merge ligand, receptor and GFP channels. Scale bars, 20 µm. Bar plots indicate the average intensity of ligands and receptors, normalized to DAPI intensity, across five images from each patient, in GBM cells (defined by GFP expression) and NPCs. Error bars indicate SEM. (B) Immunohistochemistry images show expression of NICD1 (the cleaved intracellular domain of NOTCH1), indicating NOTCH1 activation, in cryosections of monoculture and co-culture spheroids comprising NPCs and GBM cells from patients F3 or F6. Scale bars, 20 µm. Bar plots indicate the average NICD1 intensity, normalized to DAPI intensity, across two to five images per condition, in GBM cells (defined by GFP expression) and NPCs. Error bars indicate SEM. (adapted from Krieger et al., 2020)

4 Discussion

As the invasive behaviour of glioblastoma has crucial implications for disease treatment and patient outcome, a method to study this process efficiently *in vitro* offers great potential for improving our understanding of glioblastoma biology and our ability to develop targeted therapies. To overcome the limitations of previous experimental approaches, especially the reliance on murine tissues and the long timescales required for earlier *in vitro* models, we have developed a novel system to model glioblastoma invasion into iPSC-derived human brain organoids within an appropriate timeframe for clinical use. As our protocol is based on commercially available cell culture plates and media, it is highly scalable and reproducible, making it well suited to high-throughput applications.

To image the invasion of fluorescently labelled GBM cells into organoids, we employed fructose-based tissue clearing and confocal microscopy. Alternative tissue clearing protocols were tested but proved either less effective or too time-consuming without providing better clearing results. We also trialled different imaging modalities, but found that the light-sheet microscope available in our laboratory did not offer sufficient penetration depth while our two-photon imaging setup was too slow for this application. We show that, within three days, GBM cells seeded onto brain organoids extend microtubes of up to 450 μm in length, with variability between patients.

By single-cell RNA sequencing, we also detected substantial interpatient heterogeneity at the transcriptional level. Nonetheless, we could identify transcriptional changes upon co-culture of GBM with brain organoid cells that were coherent across patients, including genes with a role in neuronal migration and secretion as well as stimulus response. Our results indicate that targeting tumour microtube formation and GBM invasion might represent a therapeutic strategy with potential benefit to all GBM patients.

4.1 Context of research

Innovations in RNA sequencing technologies during the past decade have enabled the study of complex tissues at single-cell resolution. A major focus of our research group is to study how changes in transcriptional regulation correlate with morphological phenotypes. To this end, members of our laboratory are pursuing the integration of imaging and transcriptomics data through both experimental and computational advances.

The work presented in this thesis constitutes one of our first efforts to link information on cellular morphology and spatial behaviours with scRNA-seq data. In a study of breast and colorectal cancer spheroids also using the WaferGen iCell8 system, we were able to obtain transcriptional and morphological data of the same small tumour spheroids, which we correlated for an integrated study of tumour cell heterogeneity (Tirier et al., 2019). While single-cell transcriptomes and microscopy images were not derived from the same cells in the glioblastoma study, differences in invasive capacity that we observed between patient-derived GBM cell lines may point towards underlying molecular determinants of invasion. Current projects in our research group aim to establish a workflow for the visualisation of gene expression by RNA in situ hybridisation of hundreds of genes simultaneously in three-dimensional tissues; this approach could in future allow us to probe transcriptional changes in invasive GBM cells more directly using our *in vitro* model system.

Despite being one of the first scRNA-seq studies conducted in our research group, the work presented here also exemplifies a number of challenges that have resurfaced during subsequent single-cell transcriptomics investigations of different tumour entities, including colorectal carcinoma, pancreatic ductal adenocarcinoma and

lung adenocarcinoma. Most notably, these include the high degree of interpatient heterogeneity complicating cell type assignments, as well as the diversity of functional tumour cell states that partially reflect biological features of the tissue of origin.

4.2 Limitations of this work

The experimental protocol we developed to model GBM invasion has several limitations that are partly inherent in its objectives. As we were aiming for a protocol that could be realised on short timescales without relying on fetal brain tissue, our approach uses organoids that are less than one month old and therefore only provide a limited representation of the cell type diversity of the mature human brain (Renner et al., 2017). This constraint is common to many applications of iPSC-derived organoids across human tissues, and it can presently only be overcome by resorting to longer culture periods or more elaborate co-culture systems adding externally generated cell types.

Another limitation of our approach is that transcriptional changes were inferred from a mixture of GBM and organoid cells after a relatively short co-culture period of only three days. To more extensively investigate GBM invasion at the transcriptional level, it would be interesting to perform scRNA-seq on GBM cells that have invaded into mature organoids for longer time periods. By microdissection of samples prior to dissociation, one could even distinguish transcriptional changes that occur in invasive GBM cells from cells within the tumour bulk or non-invading cells at the organoid surface. However, a large number of samples would need to be processed in order to obtain sufficient numbers of invasive GBM cells.

Finally, we observed variations in invasive capacity between GBM cell lines derived from different patients, although we cannot determine with certainty based on our limited number of samples whether they reflect true heterogeneity in invasive behaviour between patients. In order to resolve this question, more GBM cell lines would need to be derived from a larger cohort. By processing more samples, one could also investigate if differences in invasive capacity relate to transcriptional characteristics of GBM cell lines in a reproducible and predictive manner.

4.3 Future research questions

While this work has demonstrated the utility of our experimental system to model glioblastoma invasion *in vitro* and study transcriptional changes induced by interactions between GBM and organoid cells, it has also highlighted several promising avenues for future research.

In addition to tracing tumour microtube formation in fixed samples, it would be very interesting to conduct long-term live imaging of the invasion process to follow the formation of an interconnected network of GBM cells in real time. As this would require an imaging approach that provides sufficient penetration depth into the tissue without prior clearing, but also high image acquisition speed and low phototoxicity, a combination of two-photon and light-sheet microscopy could be utilised for this purpose (Truong et al., 2011).

Our image analyses showed that GBM cells extend microtubes ending at other tumour cells. Additional experiments will be required to confirm whether – and at what timescales – tumour cells *in vitro* form functional connections, as previously observed *in vivo* (Osswald et al., 2015).

To arrive at a more comprehensive description of glioblastoma at the single-cell level, imaging and scRNA-seq data could also be combined with additional information, such as chromatin accessibility data (Buenrostro et al., 2015), elucidating the gene regulatory mechanisms underlying tumour invasion and cellular heterogeneity.

4.4 Clinical applications

Improvements in therapeutic outcomes for glioblastoma have been hindered by the aggressively invasive behaviour of tumour cells, as well as cellular heterogeneity between and within tumours, for decades. The association between tumour progression or invasion and the diverse functional characteristics of GBM cells, as well as their interactions with normal brain cells, remains poorly understood despite its significance for patient outcomes.

The results presented in this thesis demonstrate an experimental system for modelling and studying glioblastoma invasion *in vitro*, which may contribute to an improved understanding of this crucial feature of GBM. The initial insights gained from our scRNA-seq analyses indicate coherent transcriptional changes across patients that are implicated in GBM invasion. More detailed investigations of the gene expression signatures underlying this process could in future result in novel treatment strategies that limit GBM invasion and network formation.

Due to its reproducibility and scalability, our model system could also be used for high-throughput screens to identify drug candidates, monitoring their action on GBM and normal brain cells. As our approach uses patient-derived GBM cell lines and iPSC-derived brain organoids, such screens could in principle be conducted in a patient-specific manner.

Ultimately, the work presented here may therefore aid in the development of targeted therapies for glioblastoma and the selection of personalised treatment approaches at clinically relevant timescales.

5 References

Bian, S., Repic, M., Guo, Z., Kavirayani, A., Burkard, T., Bagley, J.A., Krauditsch, C., Knoblich, J.A., 2018. Genetically engineered cerebral organoids model brain tumor formation. Nat. Methods 15, 631–639. https://doi.org/10.1038/s41592-018-0070-7

Broekman, M.L., Maas, S.L.N., Abels, E.R., Mempel, T.R., Krichevsky, A.M., Breakefield, X.O., 2018. Multidimensional communication in the microenvirons of glioblastoma. Nat. Rev. Neurol. 14, 482–495. https://doi.org/10.1038/s41582-018-0025-8

Buenrostro, J.D., Wu, B., Litzenburger, U.M., Ruff, D., Gonzales, M.L., Snyder, M.P., Chang, H.Y., Greenleaf, W.J., 2015. Single-cell chromatin accessibility reveals principles of regulatory variation. Nature 523, 486–490. https://doi.org/10.1038/nature14590

Butler, A., Hoffman, P., Smibert, P., Papalexi, E., Satija, R., 2018. Integrating single-cell transcriptomic data across different conditions, technologies, and species. Nat. Biotechnol. 36, 411–420. https://doi.org/10.1038/nbt.4096

Camp, J.G., Sekine, K., Gerber, T., Loeffler-Wirth, H., Binder, H., Gac, M., Kanton, S., Kageyama, J., Damm, G., Seehofer, D., Belicova, L., Bickle, M., Barsacchi, R., Okuda, R., Yoshizawa, E., Kimura, M., Ayabe, H., Taniguchi, H., Takebe, T., Treutlein, B., 2017. Multilineage communication regulates human liver bud development from pluripotency. Nature 546, 533–538. https://doi.org/10.1038/nature22796

Carro, M.S., Lim, W.K., Alvarez, M.J., Bollo, R.J., Zhao, X., Snyder, E.Y., Sulman, E.P., Anne, S.L., Doetsch, F., Colman, H., Lasorella, A., Aldape, K., Califano, A., Iavarone, A., 2010. The transcriptional network for mesenchymal transformation of brain tumours. Nature 463, 318–325. https://doi.org/10.1038/nature08712

Cheng, W., Tseng, C.-J., Lin, T.T.C., Cheng, I., Pan, H.-W., Hsu, H.-C., Lee, Y.-M., 2008. Glypican-3-mediated oncogenesis involves the Insulin-like growth factor-signaling pathway. Carcinogenesis 29, 1319–1326. https://doi.org/10.1093/carcin/bgn091

Chiaradia, I., Lancaster, M.A., 2020. Brain organoids for the study of human neurobiology at the interface of in vitro and in vivo. Nat. Neurosci. 23, 1496–1508. https://doi.org/10.1038/s41593-020-00730-3

da Silva, B., Mathew, R.K., Polson, E.S., Williams, J., Wurdak, H., 2018. Spontaneous Glioblastoma Spheroid Infiltration of Early-Stage Cerebral Organoids Models Brain Tumor Invasion. SLAS Discov. 23, 862–868. https://doi.org/10.1177/2472555218764623

Darmanis, S., Sloan, S.A., Croote, D., Barres, B.A., Gephart, M.H., Quake, S.R., Darmanis, S., Sloan, S.A., Croote, D., Mignardi, M., Chernikova, S., Samghababi, P., Li, Y., Barres, B.A., Gephart, M.H., Quake, S.R., 2017. Single-Cell RNA-Seq Analysis of Infiltrating Neoplastic Cells at the Migrating Front of Human Glioblastoma. Cell Rep. 21, 1399–1410. https://doi.org/10.1016/j.celrep.2017.10.030

Eisemann, T., Costa, B., Harter, P.N., Wick, W., Mittelbronn, M., Angel, P., Peterziel, H., 2019. Podoplanin expression is a prognostic biomarker but may be dispensable for the malignancy of glioblastoma. Neuro. Oncol. 21, 326–336. https://doi.org/10.1093/neuonc/noy184

Geraldo, L.H.M., Garcia, C., da Fonseca, A.C.C., Dubois, L.G.F., de Sampaio e Spohr, T.C.L., Matias, D., de Camargo Magalhães, E.S., do Amaral, R.F., da Rosa, B.G., Grimaldi, I., Leser, F.S., Janeiro, J.M., Macharia, L., Wanjiru, C., Pereira, C.M., Moura-Neto, V., Freitas, C., Lima, F.R.S., 2019. Glioblastoma Therapy in the Age of Molecular Medicine. Trends in Cancer 5, 46–65.

https://doi.org/10.1016/j.trecan.2018.11.002

Girardot, C., Scholtalbers, J., Sauer, S., Su, S.Y., Furlong, E.E.M., 2016. Je, a versatile suite to handle multiplexed NGS libraries with unique molecular identifiers. BMC Bioinformatics 17, 4–9. https://doi.org/10.1186/s12859-016-1284-2

Goldstein, L.D., Chen, Y.J.J., Dunne, J., Mir, A., Hubschle, H., Guillory, J., Yuan, W., Zhang, J., Stinson, J., Jaiswal, B., Pahuja, K.B., Mann, I., Schaal, T., Chan, L., Anandakrishnan, S., Lin, C. wah, Espinoza, P., Husain, S., Shapiro, H., Swaminathan, K., Wei, S., Srinivasan, M., Seshagiri, S., Modrusan, Z., 2017. Massively parallel nanowell-based single-cell gene expression profiling. BMC Genomics 18, 1–10. https://doi.org/10.1186/s12864-017-3893-1

Haghverdi, L., Lun, A.T.L., Morgan, M.D., Marioni, J.C., 2018. Batch effects in single-cell RNA-sequencing data are corrected by matching mutual nearest neighbors. Nat. Biotechnol. 36, 421–427. https://doi.org/10.1038/nbt.4091

Hou, B., Zhang, D., Zhao, S., Wei, M., Yang, Z., Wang, S., Wang, J., Zhang, X., Liu, B., Fan, L., Li, Y., Qiu, Z., Zhang, C., Jiang, T., 2015. Scalable and DiI-compatible optical clearance of the mammalian brain. Front. Neuroanat. 9, 1–11. https://doi.org/10.3389/fnana.2015.00019

Humpel, C., 2015. Organotypic brain slice cultures. Neuroscience 305, 86–98. https://doi.org/10.1016/j.neuroscience.2015.07.086

Klughammer, J., Kiesel, B., Roetzer, T., Fortelny, N., Nemc, A., Nenning, K., Furtner, J., Sheffield, N.C., Datlinger, P., Peter, N., Nowosielski, M., Augustin, M., Mischkulnig, M., Ströbel, T., Alpar, D., Ergüner, B., Senekowitsch, M., Moser, P., Freyschlag, C.F., Kerschbaumer, J., Thomé, C., Grams, A.E., Stockhammer, G., Kitzwoegerer, M., Oberndorfer, S., Marhold, F., Weis, S., Trenkler, J., Buchroithner, J., Pichler, J., Haybaeck, J., Krassnig, S., Ali, K.M., von Campe, G., Payer, F., Sherif, C., Preiser, J., Hauser, T., Winkler, P.A., Kleindienst, W., Würtz, F., Brandner-Kokalj, T., Stultschnig, M., Schweiger, S., Dieckmann, K., Preusser, M., Langs, G., Baumann, B., Knosp, E., Widhalm, G., Marosi, C., Hainfellner, J.A., Woehrer, A., Bock, C., 2018. The DNA methylation landscape of glioblastoma disease progression shows extensive heterogeneity in time and space. Nat. Med. 24, 1611–1624. https://doi.org/10.1038/s41591-018-0156-x

Kobat, D., Horton, N.G., Xu, C., 2011. In vivo two-photon microscopy to 1.6-mm depth in mouse cortex. J. Biomed. Opt. 16, 106014. https://doi.org/10.1117/1.3646209

Krieger, T.G., Tirier, S.M., Park, J., Jechow, K., Eisemann, T., Peterziel, H., Angel, P., Eils, R., Conrad, C., 2020. Modeling glioblastoma invasion using human brain organoids and single-cell transcriptomics. Neuro. Oncol. 22, 1138–1149. https://doi.org/10.1093/neuonc/noaa091

Kumar, A., Wu, Y., Christensen, R., Chandris, P., Gandler, W., McCreedy, E., Bokinsky, A., Colón-Ramos, D.A., Bao, Z., McAuliffe, M., Rondeau, G., Shroff, H., 2014. Dual-view plane illumination microscopy for rapid and spatially isotropic imaging. Nat. Protoc. 9, 2555–2573. https://doi.org/10.1038/nprot.2014.172

Lancaster, M.A., Knoblich, J.A., 2014. Generation of cerebral organoids from human pluripotent stem cells. Nat. Protoc. 9, 2329–2340. https://doi.org/10.1038/nprot.2014.158

Lara-Velazquez, M., Shireman, J.M., Lehrer, E.J., Bowman, K.M., Ruiz-Garcia, H., Paukner, M.J., Chappell, R.J., Dey, M., 2021. A Comparison Between Chemo-Radiotherapy Combined With Immunotherapy and

Chemo-Radiotherapy Alone for the Treatment of Newly Diagnosed Glioblastoma: A Systematic Review and Meta-Analysis. Front. Oncol. 11, 1–16. https://doi.org/10.3389/fonc.2021.662302

Linkous, A., Balamatsias, D., Snuderl, M., Edwards, L., Miyaguchi, K., Milner, T., Reich, B., Cohen-Gould, L., Storaska, A., Nakayama, Y., Schenkein, E., Singhania, R., Cirigliano, S., Magdeldin, T., Lin, Y., Nanjangud, G., Chadalavada, K., Pisapia, D., Liston, C., Fine, H.A., 2019. Modeling Patient-Derived Glioblastoma with Cerebral Organoids. Cell Rep. 26, 3203–3211. https://doi.org/10.1016/j.celrep.2019.02.063

Mazor, T., Pankov, A., Song, J.S., Costello, J.F., 2016. Intratumoral Heterogeneity of the Epigenome. Cancer Cell 29, 440–451. https://doi.org/10.1016/j.ccell.2016.03.009

Meyer, M., Reimand, J., Lan, X., Head, R., Zhu, X., Kushida, M., Bayani, J., Pressey, J.C., Lionel, A.C., Clarke, I.D., Cusimano, M., Squire, J.A., Scherer, S.W., Bernstein, M., Woodin, M.A., Bader, G.D., Dirks, P.B., 2015. Single cell-derived clonal analysis of human glioblastoma links functional and genomic heterogeneity. Proc. Natl. Acad. Sci. 112, 851–856. https://doi.org/10.1073/pnas.1320611111

Miller, D.J., Bhaduri, A., Sestan, N., Kriegstein, A., 2019. Shared and derived features of cellular diversity in the human cerebral cortex. Curr. Opin. Neurobiol. 56, 117–124. https://doi.org/10.1016/j.conb.2018.12.005

Müller Bark, J., Kulasinghe, A., Chua, B., Day, B.W., Punyadeera, C., 2020. Circulating biomarkers in patients with glioblastoma. Br. J. Cancer 122, 295–305. https://doi.org/10.1038/s41416-019-0603-6

Neftel, C., Laffy, J., Filbin, M.G., Hara, T., Shore, M.E., Rahme, G.J., Richman, A.R., Silverbush, D., Shaw, M.L., Hebert, C.M., Dewitt, J., Gritsch, S., Perez, E.M., Gonzalez Castro, L.N., Lan, X., Druck, N., Rodman, C., Dionne, D., Kaplan, A., Bertalan, M.S., Small, J., Pelton, K., Becker, S., Bonal, D., Nguyen, Q. De, Servis, R.L., Fung, J.M., Mylvaganam, R., Mayr, L., Gojo, J., Haberler, C., Geyeregger, R., Czech, T., Slavc, I., Nahed, B. V., Curry, W.T., Carter, B.S., Wakimoto, H., Brastianos, P.K., Batchelor, T.T., Stemmer-Rachamimov, A., Martinez-Lage, M., Frosch, M.P., Stamenkovic, I., Riggi, N., Rheinbay, E., Monje, M., Rozenblatt-Rosen, O., Cahill, D.P., Patel, A.P., Hunter, T., Verma, I.M., Ligon, K.L., Louis, D.N., Regev, A., Bernstein, B.E., Tirosh, I., Suvà, M.L., 2019. An Integrative Model of Cellular States, Plasticity, and Genetics for Glioblastoma. Cell 178, 835-849.e21. https://doi.org/10.1016/j.cell.2019.06.024

Ogawa, J., Pao, G.M., Shokhirev, M.N., Verma, I.M., 2018. Glioblastoma Model Using Human Cerebral Organoids. Cell Rep. 23, 1220–1229. https://doi.org/10.1016/j.celrep.2018.03.105

Omuro, A., DeAngelis, L.M., 2013. Glioblastoma and Other Malignant Gliomas. Jama 310, 1842–1850. https://doi.org/10.1001/jama.2013.280319

Onda, K., Tanaka, R., Takahashi, H., Takeda, N., Ikuta, F., 1989. Cerebral Glioblastoma with Cerebrospinal Fluid Dissemination: A Clinicopathological Study of 14 Cases Examined by Complete Autopsy. Neurosurgery 25, 533–540.

Osswald, M., Jung, E., Sahm, F., Solecki, G., Venkataramani, V., Horstmann, H., Liao, Y., Syed, M., Blaes, J., Berghoff, A., Ratliff, M., Lemke, D., Gömmel, M., Pauli, M., Häring, P., Herl, V., Steinhäuser, C., Miletic, H., Preusser, M., Weiss, S., Liu, H., Huber, P.E., Kuner, T., von Deimling, A., Wick, W., Winkler, F., 2015. Brain tumor cells interconnect to a functional and resistant network. Nature 528, 93–98. https://doi.org/10.1038/nature16071

Patel, A.P., Tirosh, I., Trombetta, J.J., Shalek, A.K., Gillespie, S.M., Wakimoto, H., Cahill, D.P., Nahed, B. V,

Curry, W.T., Martuza, R.L., Louis, D.N., Rozenblatt-Rosen, O., Suvà, M.L., Regev, A., Bernstein, B.E., 2014. Single-cell RNA-seq highlights intratumoral heterogeneity in primary glioblastoma. Science 344, 1396–1401. https://doi.org/10.1126/science.1254257

Paw, I., Carpenter, R.C., Watabe, K., Debinski, W., Lo, H.W., 2015. Mechanisms regulating glioma invasion. Cancer Lett. 362, 1–7. https://doi.org/10.1016/j.canlet.2015.03.015

Power, R.M., Huisken, J., 2017. A guide to light-sheet fluorescence microscopy for multiscale imaging. Nat. Methods 14, 360–373. https://doi.org/10.1038/nmeth.4224

Puram, S. V., Tirosh, I., Parikh, A.S., Patel, A.P., Yizhak, K., Gillespie, S., Rodman, C., Luo, C.L., Mroz, E.A., Emerick, K.S., Deschler, D.G., Varvares, M.A., Mylvaganam, R., Rozenblatt-Rosen, O., Rocco, J.W., Faquin, W.C., Lin, D.T., Regev, A., Bernstein, B.E., 2017. Single-Cell Transcriptomic Analysis of Primary and Metastatic Tumor Ecosystems in Head and Neck Cancer. Cell 171, 1611-1624.e24. https://doi.org/10.1016/j.cell.2017.10.044

Ramilowski, J.A., Goldberg, T., Harshbarger, J., Kloppmann, E., Lizio, M., Satagopam, V.P., Itoh, M., Kawaji, H., Carninci, P., Rost, B., Forrest, A.R.R., 2015. A draft network of ligand–receptor-mediated multicellular signalling in human. Nat. Commun. 6, 7866. https://doi.org/10.1038/ncomms8866

Renner, M., Lancaster, M.A., Bian, S., Choi, H., Ku, T., Peer, A., Chung, K., Knoblich, J.A., 2017. Self-organized developmental patterning and differentiation in cerebral organoids. EMBO J. 36, 1316–1329. https://doi.org/10.15252/embj.201694700

Ricard, D., Idbaih, A., Ducray, F., Lahutte, M., Hoang-Xuan, K., Delattre, J.Y., 2012. Primary brain tumours in adults. Lancet 379, 1984–1996. https://doi.org/10.1016/S0140-6736(11)61346-9

Richardson, D.S., Lichtman, J.W., 2015. Clarifying Tissue Clearing. Cell 162, 246–257. https://doi.org/10.1016/j.cell.2015.06.067

Smith, C.L., 2011. Basic confocal microscopy. Curr. Protoc. Neurosci. Chapter 2, Unit 2.2. https://doi.org/10.1002/0471142301.ns0202s56

Sottoriva, A., Spiteri, I., Piccirillo, S.G.M., Touloumis, A., Collins, V.P., Marioni, J.C., Curtis, C., Watts, C., Tavare, S., 2013. Intratumor heterogeneity in human glioblastoma reflects cancer evolutionary dynamics. Proc. Natl. Acad. Sci. 110, 4009–4014. https://doi.org/10.1073/pnas.1219747110

Stegle, O., Teichmann, S.A., Marioni, J.C., 2015. Computational and analytical challenges in single-cell transcriptomics. Nat. Rev. Genet. 16, 133–145. https://doi.org/10.1038/nrg3833

Subramanian, A., Tamayo, P., Mootha, V.K., Mukherjee, S., Ebert, B.L., Gillette, M.A., Paulovich, A., Pomeroy, S.L., Golub, T.R., Lander, E.S., Mesirov, J.P., 2005. Gene set enrichment analysis: A knowledge-based approach for interpreting genome-wide expression profiles. Proc. Natl. Acad. Sci. 102, 15545–15550. https://doi.org/10.1073/pnas.0506580102

Suvà, M.L., Tirosh, I., 2019. Single-Cell RNA Sequencing in Cancer: Lessons Learned and Emerging Challenges. Mol. Cell 75, 7–12. https://doi.org/10.1016/j.molcel.2019.05.003

Tirier, S.M., Park, J., Preußer, F., Amrhein, L., Gu, Z., Steiger, S., Mallm, J.-P., Krieger, T., Waschow, M., Eismann, B., Gut, M., Gut, I.G., Rippe, K., Schlesner, M., Theis, F., Fuchs, C., Ball, C.R., Glimm, H., Eils, R., Conrad, C., 2019. Pheno-seq – linking visual features and gene expression in 3D cell culture systems. Sci. Rep. 9, 12367. https://doi.org/10.1038/s41598-019-48771-4

Truong, T. V., Supatto, W., Koos, D.S., Choi, J.M., Fraser, S.E., 2011. Deep and fast live imaging with two-

photon scanned light-sheet microscopy. Nat. Methods 8, 757–762. https://doi.org/10.1038/nmeth.1652

van der Maaten, L., Hinton, G., 2008. Visualizing Data using t-SNE. J. Mach. Learn. Res. 9, 2579–2605. https://doi.org/10.1007/s10479-011-0841-3

Verhaak, R.G.W., Hoadley, K.A., Purdom, E., Wang, V., Qi, Y., Wilkerson, M.D., Miller, C.R., Ding, L., Golub, T., Mesirov, J.P., Alexe, G., Lawrence, M., O'Kelly, M., Tamayo, P., Weir, B.A., Gabriel, S., Winckler, W., Gupta, S., Jakkula, L., Feiler, H.S., Hodgson, J.G., James, C.D., Sarkaria, J.N., Brennan, C., Kahn, A., Spellman, P.T., Wilson, R.K., Speed, T.P., Gray, J.W., Meyerson, M., Getz, G., Perou, C.M., Hayes, D.N., 2010. Integrated Genomic Analysis Identifies Clinically Relevant Subtypes of Glioblastoma Characterized by Abnormalities in PDGFRA, IDH1, EGFR, and NF1. Cancer Cell 17, 98–110. https://doi.org/10.1016/j.ccr.2009.12.020

Vollmann-Zwerenz, A., Leidgens, V., Feliciello, G., Klein, C.A., Hau, P., 2020. Tumor cell invasion in glioblastoma. Int. J. Mol. Sci. 21, 1–21. https://doi.org/10.3390/ijms21061932

Weil, S., Osswald, M., Solecki, G., Grosch, J., Jung, E., Lemke, D., Ratliff, M., Hänggi, D., Wick, W., Winkler, F., 2017. Tumor microtubes convey resistance to surgical lesions and chemotherapy in gliomas. Neuro. Oncol. 19, 1316–1326. https://doi.org/10.1093/neuonc/nox070

Winkler, F., Wick, W., 2018. Harmful networks in the brain and beyond. Science 359, 1100–1101. https://doi.org/10.1126/science.aar5555

Wrensch, M., Minn, Y., Chew, T., Bondy, M., Berger, M.S., 2002. Epidemiology of primary brain tumors. Neurooncology 4, 278–299. https://doi.org/10.1007/978-94-007-1706-0_1

Wu, Y., Wawrzusin, P., Senseney, J., Fischer, R.S., Christensen, R., Santella, A., York, A.G., Winter, P.W., Waterman, C.M., Bao, Z., Colón-Ramos, D.A., McAuliffe, M., Shroff, H., 2013. Spatially isotropic four-dimensional imaging with dual-view plane illumination microscopy. Nat. Biotechnol. 31, 1032–1038. https://doi.org/10.1038/nbt.2713

6 Eidesstattliche Versicherung

Ich, Teresa Gabriela Krieger, versichere an Eides statt durch meine eigenhändige Unterschrift, dass ich die vorgelegte Dissertation mit dem Thema „Modellierung der Invasion von Glioblastomen mittels Mikroskopie und Sequenzierung“ („Combined imaging and sequencing to model glioblastoma invasion“) selbstständig und ohne nicht offengelegte Hilfe Dritter verfasst und keine anderen als die angegebenen Quellen und Hilfsmittel genutzt habe.

Alle Stellen, die wörtlich oder dem Sinne nach auf Publikationen oder Vorträgen anderer Autoren/innen beruhen, sind als solche in korrekter Zitierung kenntlich gemacht. Die Abschnitte zu Methodik (insbesondere praktische Arbeiten, Laborbestimmungen, statistische Aufarbeitung) und Resultaten (insbesondere Abbildungen, Graphiken und Tabellen) werden von mir verantwortet.

Ich versichere ferner, dass ich die in Zusammenarbeit mit anderen Personen generierten Daten, Datenauswertungen und Schlussfolgerungen korrekt gekennzeichnet und meinen eigenen Beitrag sowie die Beiträge anderer Personen korrekt kenntlich gemacht habe (siehe Anteilserklärung). Texte oder Textteile, die gemeinsam mit anderen erstellt oder verwendet wurden, habe ich korrekt kenntlich gemacht.

Meine Anteile an etwaigen Publikationen zu dieser Dissertation entsprechen denen, die in der untenstehenden gemeinsamen Erklärung mit dem Erstbetreuer angegeben sind. Für sämtliche im Rahmen der Dissertation entstandenen Publikationen wurden die Richtlinien des ICMJE (International Committee of Medical Journal Editors; www.icmje.og) zur Autorenschaft eingehalten. Ich erkläre ferner, dass ich mich zur Einhaltung der Satzung der Charité – Universitätsmedizin Berlin zur Sicherung Guter Wissenschaftlicher Praxis verpflichte.

Weiterhin versichere ich, dass ich diese Dissertation weder in gleicher noch in ähnlicher Form bereits an einer anderen Fakultät eingereicht habe.

Die Bedeutung dieser eidesstattlichen Versicherung und die strafrechtlichen Folgen einer unwahren eidesstattlichen Versicherung (§§156, 161 des Strafgesetzbuches) sind mir bekannt und bewusst.

Datum Unterschrift

7 Anteilserklärung

Teresa Gabriela Krieger hatte folgenden Anteil an der folgenden Publikation:

> Krieger TG, Tirier SM, Park J, Eisemann T, Peterziel A, Angel P, Eils R, Conrad C:
> Modeling glioblastoma invasion using human brain organoids and single-cell transcriptomics,
> Neuro-Oncology, 22: 1138–1149 (2020)

Teresa Gabriela Krieger entwickelte das Studiendesign zusammen mit Christian Conrad und Roland Eils. Sie adaptierte das experimentelle Protokoll für die Generierung von zerebralen Organoiden basierend auf einer vorhergehenden Publikation und entwickelte das Protokoll für die Ko-Kultur mit GBM-Zellen. Dabei entstanden die Abbildungen 1A und 3A im Haupttext der Publikation sowie die Tabelle 1 im Anhang (‚Supplementary Material'). Außerdem führte sie die experimentellen Arbeiten durch, wobei sie teilweise durch Katharina Jechow (Technische Assistentin) bei der Zellkultur sowie durch Stephan Tirier (Doktorand) bei den Sequenzierungsschritten unterstützt wurde. Mikroskopie und Bildanalysen wurden ebenfalls von Teresa Gabriela Krieger durchgeführt. Basierend darauf generierte sie die Abbildungen 1B, 2 und 3B-C im Haupttext der Publikation sowie die Abbildungen 1, 2, 3, 4A und 7 und die Videos 1-4 im Anhang. Ausgehend von den durch Jeongbin Park präprozessierten Daten, die dann in tabellarischer Form (Zellen x Transkripte) vorlagen, analysierte sie die Transkriptom-Daten. Daraus generierte sie die Abbildungen 3D-G und 4 im Haupttext der Publikation sowie die Tabelle 2 und die Abbildungen 4B-C, 5 und 6 im Anhang. Zudem schrieb sie das Manuskript für die Publikation.

_____

Unterschrift der Doktorandin

8 Auszug aus der Journal Summary List

Journal Data Filtered By: **Selected JCR Year: 2018** Selected Editions: SCIE,SSCI
Selected Categories: **"ONCOLOGY"** Selected Category Scheme: WoS
Gesamtanzahl: 229 Journale

Rank	Full Journal Title	Total Cites	Journal Impact Factor	Eigenfactor Score
1	CA-A CANCER JOURNAL FOR CLINICIANS	32,410	223.679	0.077370
2	NATURE REVIEWS CANCER	50,529	51.848	0.074080
3	LANCET ONCOLOGY	48,822	35.386	0.146770
4	Nature Reviews Clinical Oncology	9,626	34.106	0.031890
5	JOURNAL OF CLINICAL ONCOLOGY	154,029	28.245	0.281750
6	Cancer Discovery	13,715	26.370	0.064810
7	CANCER CELL	36,056	23.916	0.091050
8	JAMA Oncology	9,488	22.416	0.048340
9	ANNALS OF ONCOLOGY	40,751	14.196	0.103620
10	Journal of Thoracic Oncology	16,601	12.460	0.038810
11	Molecular Cancer	11,626	10.679	0.021350
12	JNCI-Journal of the National Cancer Institute	36,790	10.211	0.051650
13	NEURO-ONCOLOGY	11,858	10.091	0.029150
14	LEUKEMIA	24,555	9.944	0.054750
15	SEMINARS IN CANCER BIOLOGY	6,992	9.658	0.010730
16	CLINICAL CANCER RESEARCH	78,171	8.911	0.134870
17	Trends in Cancer	1,420	8.884	0.006040
18	Journal of Hematology & Oncology	5,366	8.731	0.013620
19	Journal for ImmunoTherapy of Cancer	2,716	8.676	0.011350
20	Cancer Immunology Research	5,420	8.619	0.025380
21	CANCER RESEARCH	130,932	8.378	0.123870

9 Publikation

Krieger TG, Tirier SM, Park J, Eisemann T, Peterziel A, Angel P, Eils R, Conrad C: Modeling glioblastoma invasion using human brain organoids and single-cell transcriptomics. *Neuro-Oncology,* 22 (8): 1138–1149 (2020). https://doi.org/10.1093/neuonc/noaa091

1138

Neuro-Oncology

22(8), 1138–1149, 2020 | doi:10.1093/neuonc/noaa091 | Advance Access date 16 April 2020

Modeling glioblastoma invasion using human brain organoids and single-cell transcriptomics

Teresa G. Krieger, Stephan M. Tirier, Jeongbin Park, Katharina Jechow, Tanja Eisemann, Heike Peterziel, Peter Angel, Roland Eils, and Christian Conrad

Digital Health Center, Berlin Institute of Health and Charité, Berlin, Germany (T.G.K., J.P, K.J., R.S., C.C.); Division of Theoretical Bioinformatics, German Cancer Research Center, Heidelberg, Germany (T.G.K., J.P, K.J., R.E., C.C.); Division of Chromatin Networks, German Cancer Research Center, Heidelberg, Germany (S.M.T.); Division of Signal Transduction and Growth Control, DKFZ/ZMBH Alliance, Heidelberg, Germany (T.E., H.P, P.A.); Faculty of Biosciences, University of Heidelberg, Heidelberg, Germany (T.E.); Present affiliation: Hopp Children's Tumor Center Heidelberg and Clinical Cooperation Unit Paediatric Oncology, German Cancer Research Center, Heidelberg, Germany (H.P.); Health Data Science Unit, Faculty of Medicine, University of Heidelberg, Heidelberg, Germany (R.E.)

Corresponding Authors: Christian Conrad, Digital Health Centre, Berlin Institute of Health, Kapelle-Ufer 2, 10117 Berlin, Germany (phone: +49 30/450-543 097, fax: +49 30/450-7576902 (christian.conrad@bihealth.de); and Roland Eils, Digital Health Centre, Berlin Institute of Health, Kapelle-Ufer 2, 10117 Berlin, Germany (phone: +49 30/450-543 088, fax: +49 30/450-7576902 (roland.eils@charite.de)

Abstract

Background. Glioblastoma (GBM) consists of devastating neoplasms with high invasive capacity, which have been difficult to study in vitro in a human-derived model system. Therapeutic progress is also limited by cellular heterogeneity within and between tumors, among other factors such as therapy resistance. To address these challenges, we present an experimental model using human cerebral organoids as a scaffold for patient-derived GBM cell invasion.

Methods. This study combined tissue clearing and confocal microscopy with single-cell RNA sequencing of GBM cells before and after co-culture with organoid cells.

Results. We show that tumor cells within organoids extend a network of long microtubes, recapitulating the in vivo behavior of GBM. Transcriptional changes implicated in the invasion process are coherent across patient samples, indicating that GBM cells reactively upregulate genes required for their dispersion. Potential interactions between GBM and organoid cells identified by an in silico receptor–ligand pairing screen suggest functional therapeutic targets.

Conclusions. Taken together, our model has proven useful for studying GBM invasion and transcriptional heterogeneity in vitro, with applications for both pharmacological screens and patient-specific treatment selection on a time scale amenable to clinical practice.

Key Points

1. Organoid technology and single-cell transcriptomics reveal cellular interactions of invasive GBM cells.
2. Transcriptional changes implicated during invasion suggest novel therapeutic targets for GBM.
3. Time scales are amenable to clinical practice and high-content drug screens.

Glioblastoma (GBM) is the most frequent and most aggressive primary brain tumor.[1,2] Despite decades of intensive research, average survival time remains at 12–15 months from diagnosis.[3] Surgical resection of GBM tumors is rarely complete because the tumor aggressively infiltrates the brain, with cells interconnecting via long membrane protrusions (microtubes).[4] The resulting network enables multicellular communication through

Importance of the Study

Human induced pluripotent stem cell–derived organoids have recently emerged as biologically relevant in vitro models, while single-cell transcriptomics provides a powerful new approach for resolving gene expression at the cellular level. Here, we have combined both techniques to study cellular interactions of invasive GBM cells in human cerebral organoids. Our GBM co-culture assay successfully uncovers transcriptional changes implicated in the invasion process as well as potential ligand–receptor interactions between GBM and organoid cells, suggesting novel therapeutic targets for GBM. Our approach enables efficient quantitative studies of GBM and other invasive tumors in vitro, on time scales amenable to clinical practice and high-content drug screens.

microtube-associated gap junctions, and increases tumor resistance to cell ablation and radiotherapy.[5] Moreover, GBM cells interact with normal brain cells via soluble factors or direct cell-cell contacts to promote tumor proliferation and invasion.[6]

Two major challenges have impeded progress in the development of new GBM therapies. Firstly, there is increasing evidence for substantial genetic,[7,8] epigenetic,[9,10] and transcriptional heterogeneity[11] between and within human tumors. Recent advances in single-cell RNA sequencing (scRNA-seq) technology have enabled the transcriptomic analysis of numerous tumor entities at the level of individual cells. However, in the case of GBM, resection of primary samples has resulted in limited insight into interactions between infiltrating tumor and normal brain cells, as isolation of neoplastic cells from the tumor periphery has proven challenging.[12] How cellular heterogeneity of GBM cells and their interactions with normal brain cells relate to differences in proliferation or invasive capacity, which ultimately determine patient outcome, thus remains unknown.

A second challenge in the advancement of GBM therapies is the current lack of model systems to study defining properties of human GBM, especially invasion into the surrounding brain tissue. Previous in vitro models have suffered from limited physiological relevance or have been incompatible with the time scales for clinical decision making.[6] Recent studies have shown that human cerebral organoids can be used as a platform for tumor cell transplantation or genetic engineering of tumors, enabling microscopic observation of tumor development.[13–16] However, tumor cell interactions with normal brain cells have not been addressed yet.

Here, we developed an experimental approach to study the interaction of GBM and normal brain cells of the neuronal lineage in vitro, on clinically relevant time scales of less than 4 weeks. We used induced pluripotent stem cell (iPSC)–derived human cerebral organoids as a 3D scaffold for the invasion of patient-derived GBM cells and analyzed tumor microtube development by tissue clearing, confocal microscopy, and semi-automated quantification. In addition, we performed scRNA-seq of GBM cells before and after co-culture with organoid cells and identified a transcriptional program induced by the interactions between tumor and normal brain cells, suggesting potential therapeutic targets.

Materials and Methods

GBM Cell Culture

Primary tumor samples were received from the Edinger Institute of Frankfurt University Hospital. Informed consent was obtained prior to surgery. Experiments involving human patient material were performed in accordance with the Declaration of Helsinki and were approved by the ethics committee of the University Cancer Center Frankfurt (project #SNO-01-13). Patient-derived GBM cell cultures were established as described.[17] Cells were cultured in suspension culture in 75 cm^2 ultra-low attachment flasks in Neurobasal medium (Gibco) supplemented with 2 mM L-glutamine (Life Technologies), 1x B27 (Gibco), 2 µg/mL heparin, 20 ng/mL epidermal growth factor and 20 ng/mL basic fibroblast growth factor (R&D Systems). For passaging, spheroid cultures were dissociated using Accutase (StemCell Technologies) when they had reached diameters of ~100 µm, every 1–3 weeks. To confirm the invasive capacity of GBM cells in hydrogel matrix, spheroids were embedded in Matrigel (Corning).

Lentiviral Labeling and FACS

Second-generation replication-incompetent lentivirus was produced by FuGENE transfection (Promega) of HEK293T cells with the expression plasmid LeGO-G2, complemented with the packaging plasmids psPAX2 and pMD2.G (all from Addgene). GBM cells were infected on 3 consecutive days by spinoculation at 800g for 30–60 minutes, and green fluorescent protein (GFP)–expressing cells were isolated by fluorescence activated cell sorting (FACS). Lentivirally labeled GBM cells were maintained in neural maintenance medium and passaged every 1–3 weeks as described above.

Organoid Culture

The iPSC line 409b2 was obtained from the Riken Institute in Japan. For routine culture, iPSCs were maintained in mTeSR1 medium (StemCell Technologies) on tissue culture plates coated with Matrigel (Corning) and passaged every 4–5 days using Gentle Cell Dissociation Reagent (StemCell

Technologies). For organoid seeding, iPSCs were dissociated with Accutase (StemCell Technologies) and transferred into AggreWell plates in Neural Induction Medium (StemCell Technologies) with 10 μM Y-27632 (StemCell Technologies) at a density of 1000 cells per cavity, following manufacturers' instructions. Spheroid formation was confirmed visually after 24 hours, and spheroids were maintained in Neural Induction Medium (StemCellTechnologies) with daily medium changes. After 5 days, spheroids were harvested from the AggreWell plates and embedded in Matrigel. Medium was changed to neural maintenance medium, a 1:1 mixture of N2- and B27-containing media (N2 medium: DMEM/F12 GlutaMAX, 1 × N2, 5 μg/mL insulin, 1 mM L-glutamine, 1 × non-essential amino acids, 100 μM 2-mercaptoethanol; B27 medium: Neurobasal, 1 × B27, 200 mM L-glutamine) supplemented with 50 U/mL penicillin and 50 mg/mL streptomycin, and exchanged every 2 days. Neural induction in 2D was performed after plating dissociated iPSCs onto Matrigel-coated plates, using the same culture media.

Organoid Invasion Assays

On day 24 of culture, organoids were removed from Matrigel by incubation with Dispase (Sigma) at 37°C and transferred to individual wells of a GravityTRAP ULA Plate (PerkinElmer). Labeled GBM cells were dissociated with Accutase and added to the organoid plate in neural maintenance medium at a concentration of 1000 cells per well. Plates were centrifuged at 100g for 3 min before returning to the incubator. After 2 days, Organoids were live stained with 100 nM SiR-actin (Spirochrome). The following day, organoids were harvested, fixed in 2% paraformaldehyde for 30 min, and embedded in Matrigel for immobilization. Tissue clearing was performed following the fructose/urea/α-thioglycerol (FRUIT) protocol as described.[18] Immunohistochemistry and control invasion assays using MCF10AT spheroids grown in Matrigel or SH-SY5Y spheroids were performed as described in the Supplementary Methods. Confocal images were acquired on an LSM780 Axio Observer confocal laser scanning microscope (Zeiss) and analyzed using custom scripts in ImageJ and MatLab, as detailed in the Supplementary Methods.

Single-Cell RNA Sequencing

For scRNA-seq of GBM cell lines, cells were cultured in neural maintenance medium for 1–3 weeks after passaging, until the largest spheroids were ~100 μm in diameter. Cells were then dissociated with Accutase (StemCell Technologies), washed twice in phosphate buffered saline (PBS), and passed through a 20 μm cell strainer (PluriSelect).

For scRNA-seq of co-cultured GBM and organoid cells, neural progenitor cell (NPC) spheroids were generated by iPSC AggreWell plates as described above. After 7 days, NPC spheroids and lentivirally labeled GBM cells from separate cultures were dissociated using Accutase, mixed in a 1:1 ratio, and replated onto AggreWell plates at 1000 cells per cavity in neural maintenance medium. After 3 days, mixed spheroids were dissociated using Accutase, washed twice in PBS, and passed through a 20 μm cell strainer (PluriSelect). Cell isolation, library preparation, and analysis of scRNA-seq data were performed as described in detail in the Supplementary Methods. Briefly, RNA-seq libraries that contained at least 150 detected genes and at most 15% mitochondrial reads were selected for downstream processing. Adapting a previously published approach,[19] aggregate expression for each gene across all cells was calculated as $E_a = \log(\text{mean}[E_{j,1\ldots n}] + 1)$, where E_j is the counts-per-million expression value of the gene in cell j. Retained for analysis were 8533 genes with $E_a > 2$. Clustering and differential expression analysis were performed using the Seurat package as implemented in R.[20] Gene set enrichment analysis[21] was performed by computing overlaps between identified gene signatures and Gene Ontology (GO_C5) gene sets derived from the Molecular Signature Database (MSigDB, https://software.broadinstitute.org/gsea/msigdb). Potential receptor–ligand pairings were analyzed based on a list of 2557 previously published receptor–ligand pairs,[22] by summing for each pair of cells the number of ligand–receptor pairs potentially connecting the pair.[23]

Data Availability

Raw sequencing data have been deposited at the European Genome-Phenome Archive (https://www.ebi.ac.uk/ega/home) under accession number EGAS00001003852. Scripts used for analyzing transcriptome data and image data (in R, Fiji, and MatLab) are available from the authors upon request.

Results

Induced PSC–Derived Cerebral Organoids Provide a Scaffold for Glioblastoma Invasion

To study GBM invasion in a physiologically relevant 3D context, we adapted an established protocol for human iPSC-derived cerebral organoid development[24] to achieve streamlined and reproducible production of organoids (Supplementary Methods and Supplementary Figure 1). From 24 days of age, cerebral organoids were co-cultured with fluorescently labeled GBM cells from 4 patient-derived cell lines (Figure 1A, Supplementary Table 1, and Supplementary Figure 1). Samples were fixed after 3 days and subjected to tissue clearing using the FRUIT protocol,[18] enabling the visualization of tumor invasion by confocal microscopy. We found that tumor cells from all 4 GBM patients readily attached to and invaded into the organoids (Figure 1B). Tumor cells formed protrusions reaching to other cells over short and long distances (Figure 1B and Supplementary Figure 2A), consistent with tumor microtube formation observed in vivo in mice.[4] GBM cells primarily invaded into the neuronal layers of the organoids, with little invasion into neural progenitor rosettes (Figure 1B and Supplementary Figure 2B). Conversely, we did not observe invasion of GBM

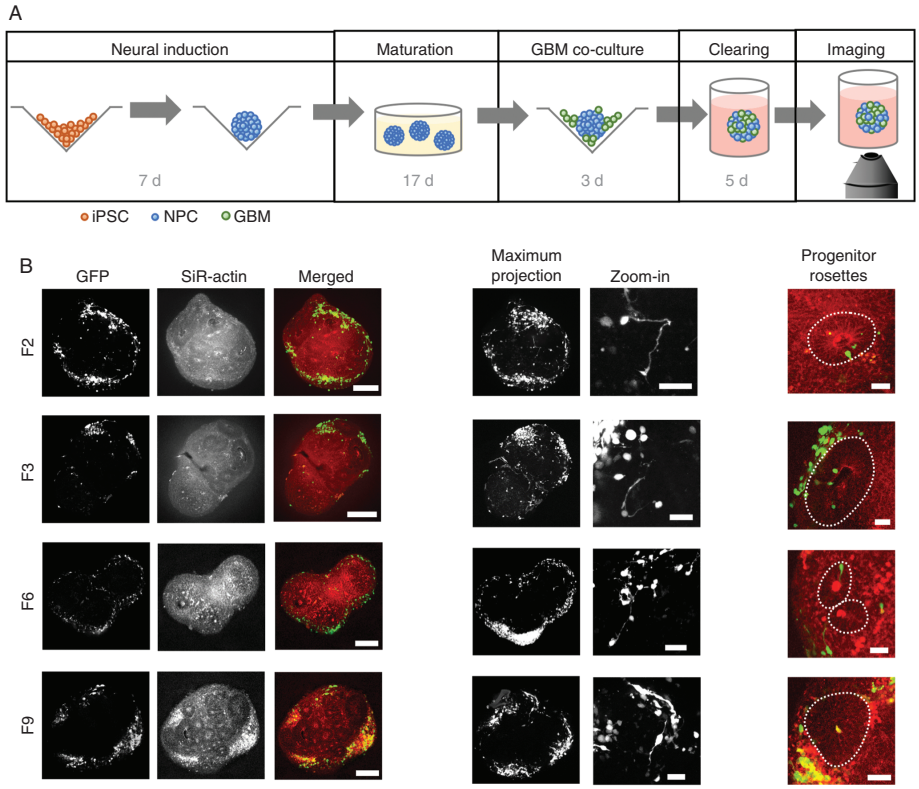

Figure 1. GBM invasion assay. (A) Experimental protocol. Following 7 days of neural induction, organoids were transferred to Matrigel and matured for 17 days. Organoids were then enzymatically released and co-cultured with GFP-labeled GBM cells for 3 days. Samples were embedded in Matrigel again for fixation, tissue clearing and confocal imaging. (B) GFP-labeled tumor cells from all 4 GBM patients invade into cerebral organoids (left; scale bars, 250 µm) where they form short-range and long-range connections (middle, maximum intensity projections over ~200–250 µm depth; scale bars, 50 µm). Invasion is largely restricted to neuronal layers, outside of neural progenitor rosettes indicated by dotted lines (right; scale bars, 50 µm).

cells into organoids grown from the breast cancer cell line MCF10AT[25] or the neuroblastoma cell line SH-SY5Y (Supplementary Figure 2C).

Tumor Microtube Formation Recapitulates In Vivo Behavior of GBM Cells

We developed a semi-automated image processing workflow to analyze the invasion process quantitatively (Figure 2A and Supplementary Methods), which we applied to a total of 66 organoids (n = 15–19 for each of the 4 patient GBM cell lines). We found that, for organoids of comparable sizes, the fraction of organoid volume taken up by tumor cells was similar across the 4 patient-derived cell lines (Figure 2B and Supplementary Figure 3A). The distribution of GBM cells within organoids was assessed by calculating the distances between GFP+ voxels across the same set of organoids. Tumor cells spread widely in all cases (Supplementary Figure 3B). To quantify invasion depth, we compared the distribution of distances of GFP+ voxels from the organoid surface across 12 similarly sized organoids for each patient-derived cell line. Invasion depths exceeded 100 µm in the majority of organoids (Figure 2C), with some cells detected at approximately 300 µm from the organoid surface. While migration depth of the most invasive cells (90th percentile of invasion depth) was uncorrelated with organoid size, we observed that cells from patients F6 and F9 were less invasive than cells from patients F2 and F3 (Figure 2D and Supplementary Videos); this suggests that the in vitro model may be able to reproduce intertumor heterogeneity in invasive behavior, although we cannot currently rule out that the observed differences in invasion depth stem from differences in 3D

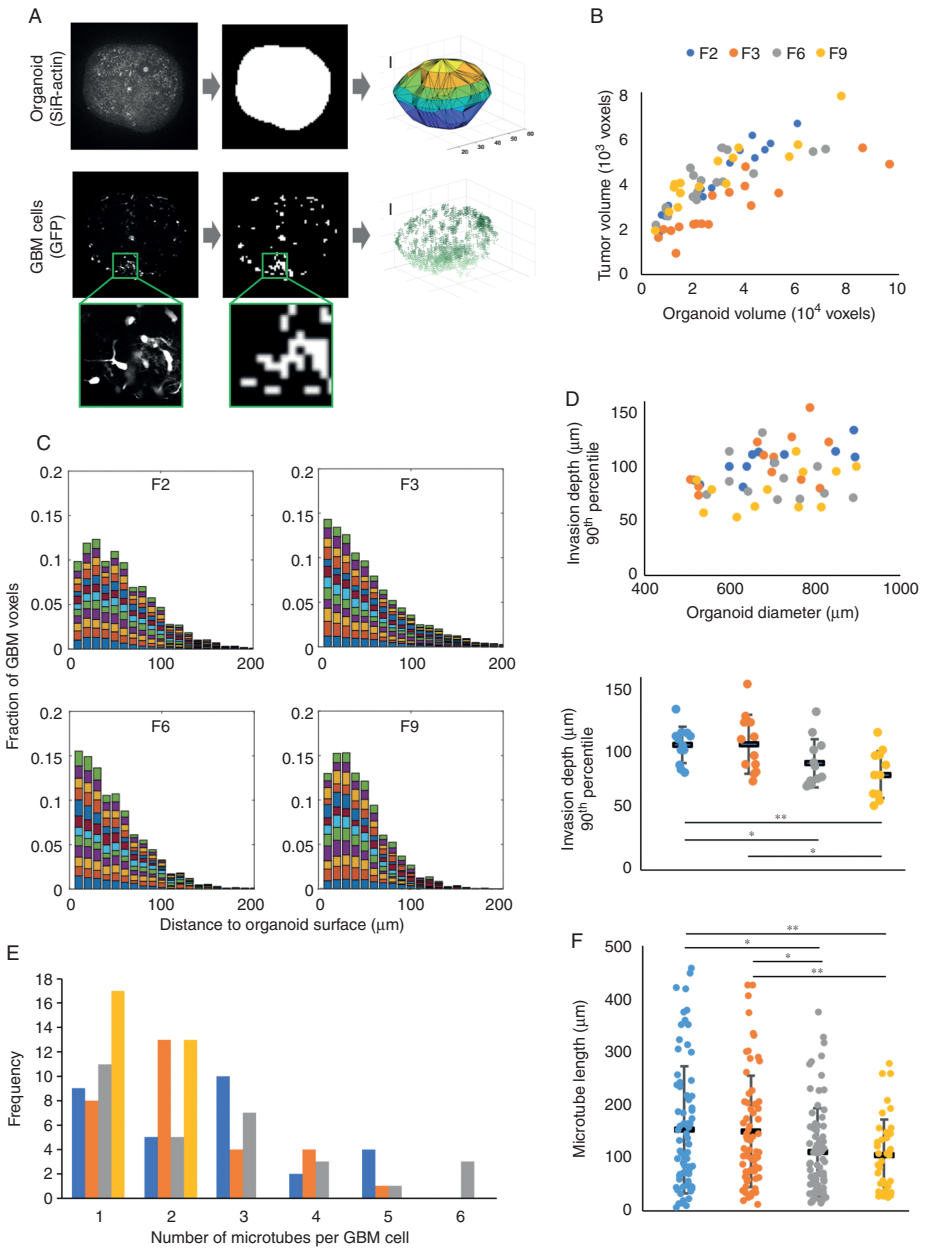

Figure 2. Morphological features of patient-derived GBM cells invading organoids. (A) Image analysis workflow. To approximate the organoid surface, organoids were incubated with the live dye SiR-actin; following fixation and clearing, the actin signal was binarized and triangulated (top). Above-threshold GFP signal was used as a proxy for GBM cell location (bottom). Scale bars, 100 µm. (B) Total tumor cell volume as a function of

architecture between the scaffold organoids. By tracing membrane-bound cellular processes in images, we found that the number of microtubes per GBM cell ranged up to 6, with 2.2 ± 0.1 microtubes on average (Figure 2E). We quantified how many of these microtubes ended at other GBM cells, and identified between 0 and 4 such putative intratumoral connections per GBM cell, with an average of 1.2 ± 0.1 connections (Supplementary Figure 3C). Individual microtubes were up to 450 µm long (Figure 2F). Consistent with our earlier observation of intertumoral heterogeneity of invasive capacity, we found that microtube lengths differed between cell lines (Figure 2F). Interestingly, the cell lines with higher invasive capacity (F2 and F3) also showed longer microtubes; this observation suggests that GBM tumors extending longer microtubes may be able to colonize organoids more efficiently in vitro, consistent with recent in vivo reports that microtubes promote tumor dissemination by allowing GBM cells to exchange cytoplasmic molecules and even translocate nuclei over long distances.[4,26]

Single-Cell RNA Sequencing Reveals Transcriptional Heterogeneity Between Tumors and After Co-Culture with Organoid Cells

Our imaging results confirm that iPSC-derived cerebral organoids represent an effective model system for quantifying GBM invasion and tumor microtube formation in vitro. To further study heterogeneity of and interactions between GBM and organoid cells at the transcriptome level, we developed a more efficient workflow that could be applied on clinically relevant time scales and at higher throughput. In the modified assay, dissociated 7-day-old cerebral organoids were mixed with GBM cells from separate cultures at a 1:1 ratio and grown in co-culture for 3 days (Figure 3A). GBM cells from all 4 patient-derived cell lines readily mixed with dissociated organoid cells (Figure 3B and Supplementary Figure 4A). With or without addition of GBM cells, dissociated organoid cells efficiently reestablished the characteristic architecture of progenitor rosettes and neuronal layers observed in cerebral organoids, and membrane protrusions emanating from tumor cells were visible in all samples (Figure 3C). After 3 days of co-culture, mixed spheroids were dissociated and subjected to scRNA-seq. For comparison, we also dissociated and sequenced recomposed spheroids of organoid cells that had not been mixed with GBM cells (ie, NPCs) below, and GBM cells from all 4 patient-derived cell lines that had been grown separately as spheroids in the same culture medium (Figure 3A). Following preprocessing and quality control, we obtained 5083 single-cell transcriptional profiles with approximately 1400 genes detected per cell on average (Supplementary Figure 4B).

Principal component analysis (PCA)–based clustering and 2D visualization by *t*-distributed stochastic neighbor embedding (t-SNE) maps revealed that GBM cells cultured alone clustered separately for each patient (clusters 5, 6, 7, and 9), confirming intertumoral heterogeneity (Figure 3D). This was also highlighted by differential expression of putative marker genes for GBM subtypes[27] across patient samples (Supplementary Figure 4C). In agreement with previous scRNA-seq studies of GBM,[11,28] we detected heterogeneous expression of gene signatures defining the classical, mesenchymal, neural, and proneural GBM subtypes[29] within each patient-derived cell line, indicating that they comprise cells most representative of more than one subtype (Supplementary Figure 5). On average, cells from patients F2 and F3 mostly corresponded to the mesenchymal subtype, while cells from patients F6 and F9 most closely matched the neural subtype; as the mesenchymal subtype has been characterized as the most invasive,[29,30] this is consistent with our earlier observation that F2 and F3 display higher invasive capacity in vitro.

We further identified 3 clusters (clusters 0, 1, and 3) containing cells from the unmixed organoids as well as cells from all 4 mixed samples, and concluded that the latter represent the organoid cells in the mixed samples (Figure 3D). The remaining clusters (2, 4, and 8) contain GBM cells from patients F2, F3, and F9 after co-culture with organoid cells. Note that as only 6 such cells were identified in the mixed sample from patient F6, they were excluded from further analyses and not displayed here.

Mixing GBM and Organoid Cells Leads to Upregulation of a Shared Set of Genes Across Patients

Differential gene expression testing between GBM cell clusters from mixed and unmixed samples revealed hundreds of genes that were significantly up- or downregulated upon co-culture with organoid cells (adjusted $P < 0.05$, log(fold change) > 0.15), and an overlap of 45 genes that were upregulated in all patients (Figure 3E). These included the homeobox transcription factor PAX6 (paired box 6), normally expressed in forebrain neural stem cells; the gap junction protein alpha 1 (GJA1) coding for connexin-43, which connects tumor microtubes in GBM[4]; glypican-3 (GPC3), a cell surface heparan sulfate proteoglycan and Wnt activator whose expression correlates with invasiveness of hepatocellular carcinoma[31]; collagen COL4A5, an extracellular matrix constituent; and several lysosomal, vesicular, and secretory proteins (Figure 3F and Supplementary Table 2). Gene set enrichment analysis of the 45 coherently upregulated genes confirmed that genes relating to growth regulation, neuronal migration, extracellular secretion, and stimulus response were enriched in this group (Figure 3G). Our results thus show that interactions between GBM and organoid cells increase expression of genes required for GBM network formation and

organoid volume. (C) Distributions of distances of tumor voxels from the organoid surface of 12 organoids from each patient cell line with 500–900 µm diameter; each color represents one organoid. (D) Invasion depth of the most invasive cells from each cell line (90th percentile) compared with organoid size (top) and differences in invasion depth between patient cell lines (bottom; $*P < 0.05$, $**P < 0.01$, two-sided Student's *t*-test). (E) Number of tumor microtubes per cell observed across 30 GBM cells from each patient. (F) Microtube lengths ranged up to almost 450 µm, with GBM cells from patients F2 and F3 developing longer microtubes than cells from patients F6 and F9 ($*P < 0.05$, $**P < 0.01$, two-sided Student's *t*-test). In (D) and (F), black horizontal bars indicate mean values and error bars represent standard errors in the mean.

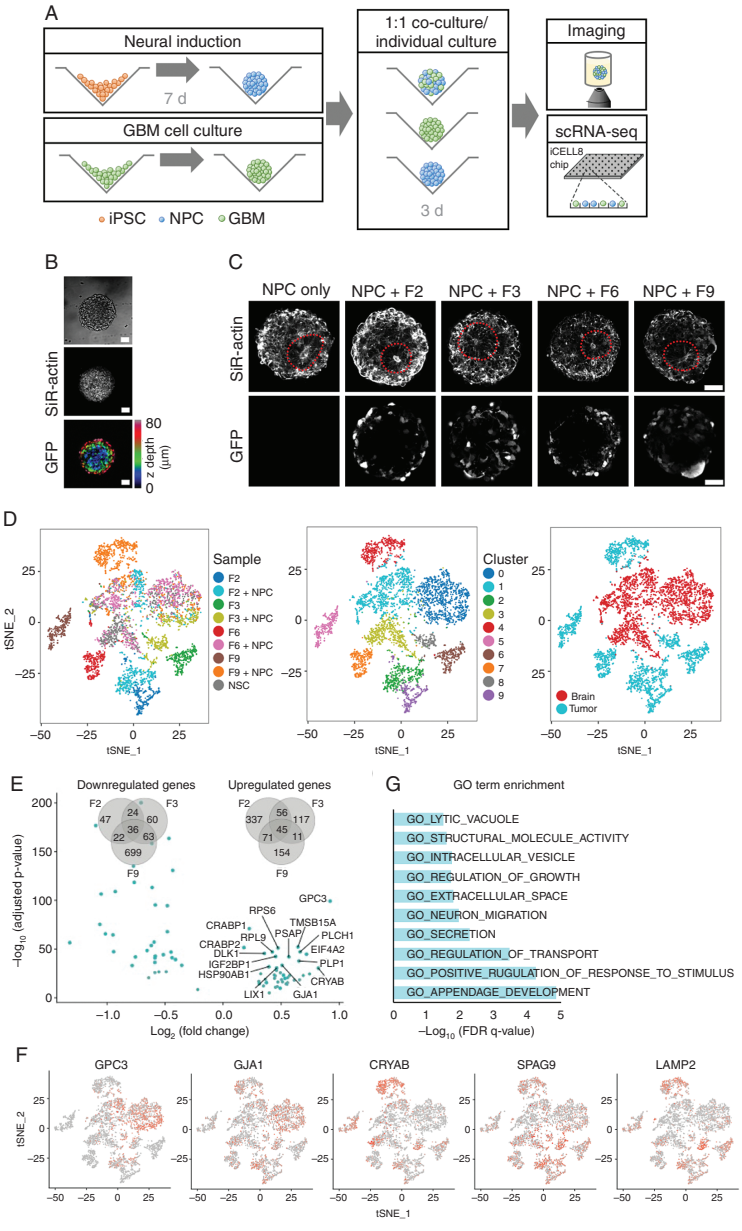

Figure 3. Single-cell RNA-seq analysis of GBM cell interactions with cerebral organoid cells. (A) Protocol for the RNA-seq experiments. Following 7 days of neural induction, organoids and spheroids of lentivirally labeled GBM cells grown separately were enzymatically dissociated and mixed at a 1:1 ratio. After 3 days of co-culture, mixed spheroids were subjected to imaging or scRNA-seq using the iCell8 system. (B) Tumor cells mixed

invasion. Comparing our results with 4 distinct cell states identified in a recent scRNA-seq study of primary GBM,[28] we noted a consistent shift in cell state composition toward a neural cell–like state in cells from patients F2 and F3 (Supplementary Figure 6).

Potential Ligand–Receptor Interactions Between Tumor Cells and Organoid Cells

To investigate the nature of interactions between GBM and organoid cells, we considered the expression of 2,557 known ligand–receptor pairs[22] across our samples, comprising a total of 1398 unique genes. Of these, 317 genes were expressed in our data, with approximately 13% expressed differentially between the same cell types in unmixed and mixed samples (Figure 4A).

Calculating the number of potential interactions between brain and tumor cells based on the expression of complementary receptors and ligands, we detected substantial crosstalk between cell types (Figure 4B). Hierarchical clustering of the number of cells potentially linked by each ligand–receptor pair revealed a group of ligand–receptor pairs that were expressed at low levels in the tumor-only and NPC-only cultures but presented many potential interactions between tumor cells and organoid cells in the mixed cultures (Figure 4C). These included several collagen-integrin interactions, GPC3 binding to insulin-like growth factor 1 receptor (IGF1R) or the cell cycle regulator CD81, and noncanonical Notch signaling (delta-like noncanonical notch ligand 1 [DLK1]/Notch 1, DLK1/Notch 2). Notably, despite the transcriptional heterogeneity we observed between patients, our approach detected consistently expressed potential interactions across all patient cell lines (Figure 4C and Supplementary Figure 7). Gene set enrichment analysis showed that the ligand–receptor pairs expressed at high levels in co-cultured samples are enriched for invasion-related genes (Figure 4D). Specifically, putative interactions in which GBM cells present the ligand and NPCs the receptor are enriched for genes involved in neuron projection development and receptor binding, whereas ligand–receptor pairs communicating in the opposite direction are enriched for extracellular matrix proteins.

Discussion

Despite its enormous therapeutic and prognostic significance, efficient methods to characterize the process of GBM invasion into human brain at a quantitative or transcriptional level are currently lacking. In this study, we present an in vitro model system in which lentivirally labeled patient-derived GBM cells invade into human cerebral organoids. By tissue clearing and confocal imaging, our approach shows that tumor cells extend up to 450 µm long membrane-bound processes after 3 days of invasion, recapitulating the development of GBM microtubes that has been observed in resected primary tumors and replicated in vivo in mice.[4] Many of these processes terminate at distant tumor cells in our in vitro model, consistent with the development of an interconnected GBM network. By making GBM invasion experimentally accessible in vitro in a 3D tissue-like architecture, our experimental approach also enables the correlation of morphological phenotypes with transcriptional regulation by integration of imaging with single-cell sequencing. Here, scRNA-seq analysis of GBM and organoid cells separately or after co-culture revealed transcriptional changes induced by the interactions of tumor cells with their environment. Genes implicated in stimulus response, neuronal migration, secretion, and extracellular matrix were coherently upregulated across all tumor samples when mixed with NPCs, indicating that GBM cells sense the presence of neuronal cells and reactively amplify the transcription of genes supporting their dispersion. Among the upregulated genes was GJA1 (coding for connexin-43), known to enable multicellular communication via gap junctions in GBM networks in vivo.[4]

Heterogeneity between and within GBM tumors has impeded therapeutic progress for decades,[32] with no targeted therapy available yet.[33] Consistently, our imaging data suggest that GBM cells from different patients vary in their invasive capacity, although future studies should confirm differences in invasive capacity between GBM cell lines within the same organoids. While additional patient samples and more single-cell transcriptional profiles would be necessary to robustly link intertumoral differences in invasion behavior with specific transcriptional changes, our results corroborated the high degree of transcriptional heterogeneity between patients.[11] However, we also detected a coherent element of transcriptional changes upon GBM and organoid cell co-culture indicating that targeting functional processes such as tumor microtube formation might improve therapeutic outcomes across patients.

Our analysis of ligand–receptor pair expression identified candidate pairs that may contribute to the invasion process, many of which have been linked with GBM progression by previous work. Glutathione S-transferase P has been shown to bind tumor necrosis factor receptor–associated factor 2 in vivo and in vitro, attenuating tumor necrosis factor signaling and thus enhancing resilience in tumor cells.[34] Notch receptors 1 and 2 are known to associate with the

efficiently with organoid cells (see also Supplementary Figure 4). Scale bars, 50 µm. (C) With or without addition of GBM cells, dissociated organoid cells reestablished the characteristic 3D architecture of neural rosettes within 3 days. Scale bars, 50 µm. (D) t-SNE map showing all cells after quality control and PCA-based clustering, colored by sample origin (left), by cluster (middle), and by organoid or tumor cell identity (right). In addition to 3 clusters containing organoid cells, GBM cells clustered separately for each patient and before or after co-culture with organoid cells. (E) Volcano plot shows the 45 genes significantly up- or downregulated across all 3 patient-derived GBM cell lines upon co-culture with organoid cells (adjusted $P < 0.05$ for each patient separately). Venn diagrams quantify the overlap of differentially regulated genes detected from each patient. (F) Expression of differentially regulated genes visualized on a t-SNE map of all cells (t-SNE representation identical to panel D). (G) Gene Ontology–based gene set enrichment analysis of genes upregulated in all patient tumor cell lines upon co-culture with organoid cells.

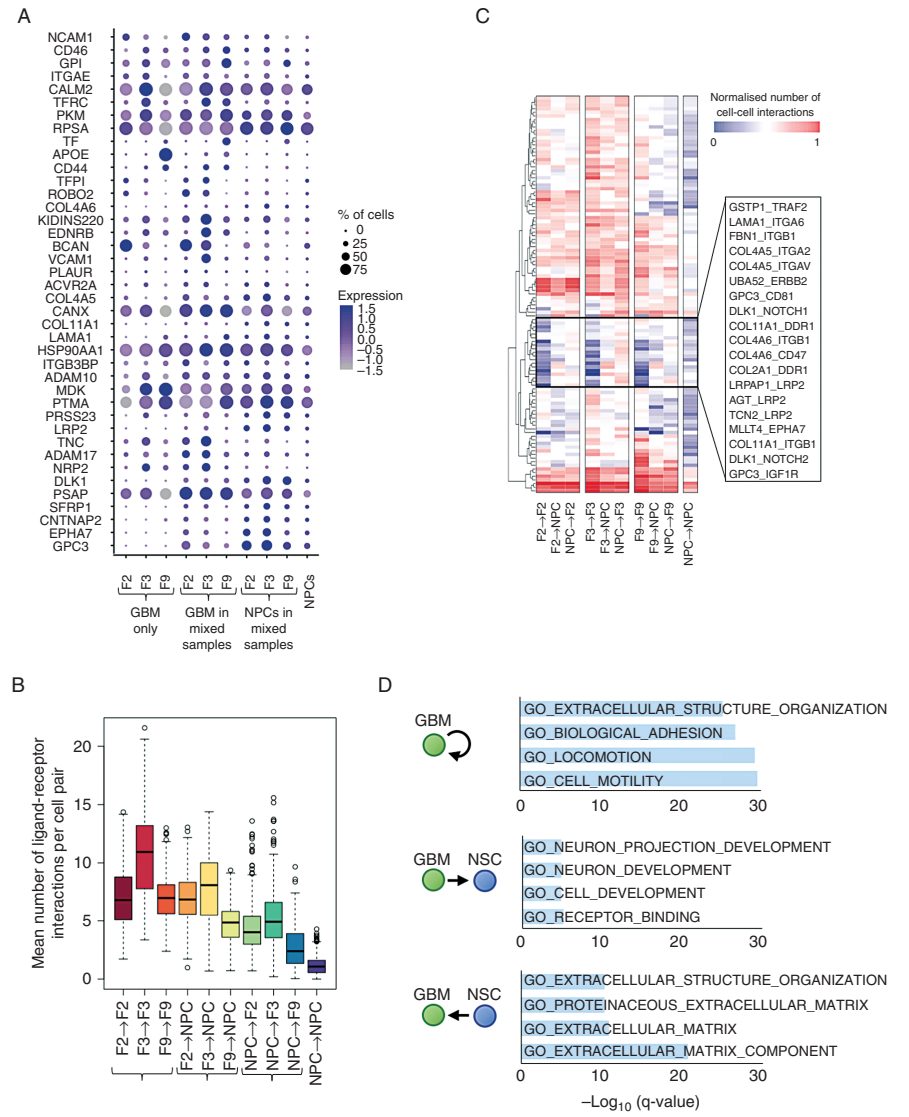

Figure 4. Potential ligand–receptor interactions between GBM and organoid cells. (A) Expression of ligand and receptor genes that are significantly upregulated in NPCs or in at least one GBM cell line upon co-culture (adjusted $P < 0.05$), averaged across GBM-only samples (left), GBM cells, or NPCs within mixed samples (middle), and the NPCs-only sample (right). Dot size corresponds to the fraction of cells expressing the gene in each group; dot color represents the average expression level. (B) The mean number of ligand–receptor pairs potentially connecting cells pairs of the given cell types, based on RNA expression levels across GBM-only samples (left), GBM cells, or NPCs within mixed samples (middle), and the NPCs-only sample (right). Center line, median; box limits, upper and lower quartiles; whiskers, 1.5x interquartile range; points, outliers. (C) Mean number of cell-cell interactions for different cell type combinations and selected ligand–receptor pairs. Hierarchical clustering reveals a group of ligand–receptor pairs (middle box) that are expressed at low levels in GBM cells or NPCs alone, but are upregulated upon co-culture. (D) Gene Ontology–based gene set enrichment analysis of ligand–receptor pairs preferentially expressed in the given cell type combinations.

transmembrane protein DLK1, but downstream effects in GBM remain unclear and may depend on heterogeneous cell states within the tumor.[35] Binding of collagens to integrins, integrin-associated protein CD47, or discoidin domain receptor tyrosine kinase 1 all correlate with GBM proliferation and invasion.[36–39] Integrin α6 as a receptor for the extracellular matrix protein laminin has also been detected in patient specimens of GBM and contributes to cancer stem cell proliferation in vitro.[40]

In addition to confirming these established signaling interactions, our in silico screen suggests putative interactions which may provide novel therapeutic targets for GBM. Binding of GPC3 to IGF1R or CD81 is known to contribute to hepatocellular carcinoma development and invasiveness[41]; immunotherapies targeting GPC3, which are showing promise in hepatocellular carcinoma,[42,43] may also benefit GBM patients. Our results also suggest AFDN/MLLT4 (adherens junction formation factor/myeloid/lymphoid or mixed-lineage leukemia) as a ligand activating ephrin receptor A7, which has been linked to adverse outcome in primary and recurrent GBM.[44] Finally, to our knowledge, the significance of fibrillin-integrin binding or of the low-density lipoprotein receptor related protein 2 interactions we detected have not been explored in GBM, but might present therapeutic opportunities. Further studies should explore the functional significance of these putative interactions.

Progress in organoid technology has led to the development of several organoid-based in vitro models for GBM within the past 2 years. Two studies have demonstrated that introducing oncogenic mutations in cerebral organoids initiates tumorigenesis,[13,14] providing a model for studying the biological mechanisms underlying GBM formation and progression. Linkous et al recently showed that patient-derived GBM cells can invade, proliferate, and form microtubes within mature, 1–5 months old cerebral organoids,[16] while da Silva et al demonstrated the feasibility of using younger organoids as a scaffold for GBM cell invasion.[15] An earlier model used GBM invading into macroscopic human engineered neural tissue, with microarray data suggesting upregulation of extracellular matrix related transcription in one GBM cell line.[45,46] Our study extends these findings to early-stage organoids generated by a highly reproducible and scalable protocol, thus enabling accelerated high-throughput screens. In contrast to previous studies, we also provide a transcriptomic characterization at the single-cell level of the GBM cell response to surrounding cerebral organoid cells.

Our results thus confirm the biological relevance of organoid-based model systems and show that interactions between GBM and organoid cells result in transcriptional changes detected by scRNA-seq. As our aim was to develop an experimental system suitable for high-throughput screens, we used organoids at 7 and 24 days of neural induction and performed scRNA-seq after just 3 days of co-culture; this potentially limits the accuracy of our results, since other cell types such as mature astrocytes are not represented in our organoids, and we cannot rule out that the transcriptional changes observed are at least partly transient reactions to being placed into co-culture.

In the future, we expect that our approach will further enable functional studies of GBM invasion that would be difficult or impossible to be conducted in vivo, including long-term imaging of network formation and multicellular communication. While we here used tissue clearing and confocal imaging for an endpoint quantification of tumor invasion, GBM-invaded organoids are similarly amenable to live imaging by two-photon or light-sheet microscopy. By combining imaging with recent single-cell RNA sequencing methodologies that provide transcriptome data for greater cell numbers,[20,47] and with other single-cell sequencing modalities such as chromatin accessibility sequencing,[48] our model could thus help resolve the functional, transcriptional, and epigenetic factors associated with different invasion behaviors of GBM or other tumors into human brain. It also provides the basis for high-content drug screens to assess patient-specific drug action on tumor and healthy brain cells, thus helping to identify the most effective drug at clinically relevant time scales.

Supplementary Material

Supplementary data are available at *Neuro-Oncology* online.

Keywords

glioblastoma | organoids | single-cell RNA sequencing | tumor cell heterogeneity | tumor invasion

Funding

This work was supported by the Bundesministerium für Bildung und Forschung (BMBF; Federal Ministry of Education and Research); Heidelberg School of Oncology (postdoctoral fellowship to TGK); PhD stipends. SMT and TE were supported by the PhD program of the Helmholtz International Graduate School for Cancer Research (PhD fellowships to SMT, TE).

Acknowledgments

The authors would like to thank Katharina Jechow for technical laboratory support, Jay Gopalakrishnan and Elke Gabriel for helpful discussions, and Monika Langlotz for FACS assistance.

Conflict of interest statement. The authors declare that they have no competing interests.

Authorship statement. Study design: TGK, CC, and RE. Protocol development for GBM invasion into cerebral organoids: TGK. Experimental work: TGK, SMT, and KJ. Data analysis: TGK and JP. Establishment of GBM cell cultures: TE, HP, and PA. Manuscript preparation: all authors.

References

1. Ricard D, Idbaih A, Ducray F, Lahutte M, Hoang-Xuan K, Delattre JY. Primary brain tumours in adults. *Lancet*. 2012;379(9830):1984–1996.
2. Omuro A, DeAngelis LM. Glioblastoma and other malignant gliomas: a clinical review. *JAMA*. 2013;310(17):1842–1850.
3. Aldape K, Brindle KM, Chesler L, et al. Challenges to curing primary brain tumours. *Nat Rev Clin Oncol*. 2019;16(8):509–520.
4. Osswald M, Jung E, Sahm F, et al. Brain tumour cells interconnect to a functional and resistant network. *Nature*. 2015;528(7580):93–98.
5. Weil S, Osswald M, Solecki G, et al. Tumor microtubes convey resistance to surgical lesions and chemotherapy in gliomas. *Neuro Oncol*. 2017;19(10):1316–1326.
6. Broekman ML, Maas SLN, Abels ER, Mempel TR, Krichevsky AM, Breakefield XO. Multidimensional communication in the microenvirons of glioblastoma. *Nat Rev Neurol*. 2018;14(8):482–495.
7. Meyer M, Reimand J, Lan X, et al. Single cell-derived clonal analysis of human glioblastoma links functional and genomic heterogeneity. *Proc Natl Acad Sci U S A*. 2015;112(3):851–856.
8. Sottoriva A, Spiteri I, Piccirillo SG, et al. Intratumor heterogeneity in human glioblastoma reflects cancer evolutionary dynamics. *Proc Natl Acad Sci U S A*. 2013;110(10):4009–4014.
9. Klughammer J, Kiesel B, Roetzer T, et al. The DNA methylation landscape of glioblastoma disease progression shows extensive heterogeneity in time and space. *Nat Med*. 2018;24(10):1611–1624.
10. Mazor T, Pankov A, Song JS, Costello JF. Intratumoral heterogeneity of the epigenome. *Cancer Cell*. 2016;29(4):440–451.
11. Patel AP, Tirosh I, Trombetta JJ, et al. Single-cell RNA-seq highlights intratumoral heterogeneity in primary glioblastoma. *Science*. 2014;344(6190):1396–1401.
12. Darmanis S, Sloan SA, Croote D, et al. Single-cell RNA-seq analysis of infiltrating neoplastic cells at the migrating front of human glioblastoma. *Cell Rep*. 2017;21(5):1399–1410.
13. Ogawa J, Pao GM, Shokhirev MN, Verma IM. Glioblastoma model using human cerebral organoids. *Cell Rep*. 2018;23(4):1220–1229.
14. Bian S, Repic M, Guo Z, et al. Genetically engineered cerebral organoids model brain tumor formation. *Nat Methods*. 2018;15(8):631–639.
15. da Silva B, Mathew RK, Polson ES, Williams J, Wurdak H. Spontaneous glioblastoma spheroid infiltration of early-stage cerebral organoids models brain tumor invasion. *SLAS Discov*. 2018;23(8):862–868.
16. Linkous A, Balamatsias D, Snuderl M, et al. Modeling patient-derived glioblastoma with cerebral organoids. *Cell Rep*. 2019;26(12):3203–3211.e5.
17. Eisemann T, Costa B, Harter PN, et al. Podoplanin expression is a prognostic biomarker but may be dispensable for the malignancy of glioblastoma. *Neuro Oncol*. 2019; 21(3):326–336.
18. Hou B, Zhang D, Zhao S, et al. Scalable and Dil-compatible optical clearance of the mammalian brain. *Front Neuroanat*. 2015;9:19.
19. Puram SV, Tirosh I, Parikh AS, et al. Single-cell transcriptomic analysis of primary and metastatic tumor ecosystems in head and neck cancer. *Cell*. 2017;171(7):1611–1624.e24.
20. Macosko EZ, Basu A, Satija R, et al. Highly parallel genome-wide expression profiling of individual cells using nanoliter droplets. *Cell*. 2015;161(5):1202–1214.
21. Subramanian A, Tamayo P, Mootha VK, et al. Gene set enrichment analysis: a knowledge-based approach for interpreting genome-wide expression profiles. *Proc Natl Acad Sci U S A*. 2005;102(43):15545–15550.
22. Ramilowski JA, Goldberg T, Harshbarger J, et al. A draft network of ligand-receptor-mediated multicellular signalling in human. *Nat Commun*. 2015;6:7866.
23. Camp JG, Sekine K, Gerber T, et al. Multilineage communication regulates human liver bud development from pluripotency. *Nature*. 2017;546(7659):533–538.
24. Lancaster MA, Knoblich JA. Generation of cerebral organoids from human pluripotent stem cells. *Nat Protoc*. 2014;9(10):2329–2340.
25. Dawson PJ, Wolman SR, Tait L, Heppner GH, Miller FR. MCF10AT: a model for the evolution of cancer from proliferative breast disease. *Am J Pathol*. 1996;148(1):313–319.
26. Winkler F, Wick W. Harmful networks in the brain and beyond. *Science*. 2018;359(6380):1100–1101.
27. Ludwig K, Kornblum HI. Molecular markers in glioma. *J Neurooncol*. 2017;134(3):505–512.
28. Neftel C, Laffy J, Filbin MG, et al. An integrative model of cellular states, plasticity, and genetics for glioblastoma. *Cell*. 2019;178(4):835–849.e21.
29. Verhaak RG, Hoadley KA, Purdom E, et al; Cancer Genome Atlas Research Network. Integrated genomic analysis identifies clinically relevant subtypes of glioblastoma characterized by abnormalities in PDGFRA, IDH1, EGFR, and NF1. *Cancer Cell*. 2010;17(1):98–110.
30. Carro MS, Lim WK, Alvarez MJ, et al. The transcriptional network for mesenchymal transformation of brain tumours. *Nature*. 2010;463(7279):318–325.
31. Cheng W, Tseng CJ, Lin TT, et al. Glypican-3-mediated oncogenesis involves the Insulin-like growth factor-signaling pathway. *Carcinogenesis*. 2008;29(7):1319–1326.
32. Reardon DA, Wen PY. Glioma in 2014: unravelling tumour heterogeneity—implications for therapy. *Nat Rev Clin Oncol*. 2015;12(2):69–70.
33. Touat M, Idbaih A, Sanson M, Ligon KL. Glioblastoma targeted therapy: updated approaches from recent biological insights. *Ann Oncol*. 2017;28(7):1457–1472.
34. Wu Y, Fan Y, Xue B, et al. Human glutathione S-transferase P1-1 interacts with TRAF2 and regulates TRAF2-ASK1 signals. *Oncogene*. 2006;25(42):5787–5800.
35. Teodorczyk M, Schmidt MHH. Notching on cancer's door: Notch signaling in brain tumors. *Front Oncol*. 2014;4:341.
36. Yamanaka R, Arao T, Yajima N, et al. Identification of expressed genes characterizing long-term survival in malignant glioma patients. *Oncogene*. 2006;25(44):5994–6002.
37. Gritsenko PG, Friedl P. Adaptive adhesion systems mediate glioma cell invasion in complex environments. *J Cell Sci*. 2018;131(15):1–11.
38. Gritsenko PG, Ilina O, Friedl P. Interstitial guidance of cancer invasion. *J Pathol*. 2012;226(2):185–199.
39. Egeblad M, Rasch MG, Weaver VM. Dynamic interplay between the collagen scaffold and tumor evolution. *Curr Opin Cell Biol*. 2010;22(5):697–706.
40. Lathia JD, Gallagher J, Heddleston JM, et al. Integrin alpha 6 regulates glioblastoma stem cells. *Cell Stem Cell*. 2010;6(5):421–432.
41. Wu Y, Liu H, Ding H. GPC-3 in hepatocellular carcinoma: current perspectives. *J Hepatocell Carcinoma*. 2016;3:63–67.
42. Dargel C, Bassani-Sternberg M, Hasreiter J, et al. T cells engineered to express a T-cell receptor specific for glypican-3 to recognize and kill hepatoma cells in vitro and in mice. *Gastroenterology*. 2015;149(4):1042–1052.

43. Wu Q, Pi L, Le Trinh T, et al. A novel vaccine targeting glypican-3 as a treatment for hepatocellular carcinoma. *Mol Ther.* 2017;25(10):2299–2308.
44. Wang LF, Fokas E, Bieker M, et al. Increased expression of EphA2 correlates with adverse outcome in primary and recurrent glioblastoma multiforme patients. *Oncol Rep.* 2008;19(1):151–156.
45. Nayernia Z, Turchi L, Cosset E, et al. The relationship between brain tumor cell invasion of engineered neural tissues and in vivo features of glioblastoma. *Biomaterials.* 2013;34(33):8279–8290.
46. Cosset E, Petty T, Dutoit V, et al. Human tissue engineering allows the identification of active miRNA regulators of glioblastoma aggressiveness. *Biomaterials.* 2016;107:74–87.
47. Zheng GX, Terry JM, Belgrader P, et al. Massively parallel digital transcriptional profiling of single cells. *Nat Commun.* 2017;8:14049.
48. Buenrostro JD, Giresi PG, Zaba LC, Chang HY, Greenleaf WJ. Transposition of native chromatin for fast and sensitive epigenomic profiling of open chromatin, DNA-binding proteins and nucleosome position. *Nat Methods.* 2013;10(12):1213–1218.

10 Lebenslauf

Mein Lebenslauf wird aus datenschutzrechtlichen Gründen in der elektronischen Version meiner Arbeit nicht veröffentlicht.

11 Publikationsliste

(IF = Impact Factor; * markiert geteilte Erstautorschaft)

2021 Zowada MK*, Tirier SM*, Dieter SM*, Krieger TG, Oberlack A, Chua RL, Huerta M, Ten FW, Laaber K, Park J, Jechow K, Müller T, Kalxdorf M, Kriegsmann M, Kriegsmann K, Herbst F, Krijgsveld J, Schneider M, Eils R, Glimm H, Conrad C, Ball CR: Functional states in tumour-initiating cell differentiation in human colorectal cancer. *Cancers*, 13 (5): 1097. *IF 6.6*

2020 Trump S*, Lukassen S*, Anker MS*, Chua RL*, Liebig J*, Thürmann L*, Corman VM, Binder M, Loske J, Klasa C, Krieger TG, Hennig BP, Messingschlager M, Pott F, Kazmierski J, Twardziok S, Albrecht JP, Eils J, Hadzibegovic S, Lena A, Heidecker B, Bürgel T, Steinfeldt J, Goffinet C, Kurth F, Witzenrath M, Völker MT, Müller SD, Liebert UG, Ishaque N, Kaderali L, Sander LE, Drosten C, Laudi S, Eils R, Conrad C, Landmesser U, Lehmann I: Hypertension delays viral clearance and exacerbates airway hyperinflammation in patients with COVID-19. *Nature Biotechnology*, doi.org/10.1038/s41587-020-00796-1. *IF 36.6*

Krieger TG, Tirier SM, Park J, Eisemann T, Peterziel A, Angel P, Eils R, Conrad C: Modeling glioblastoma invasion using human brain organoids and single-cell transcriptomics. *Neuro-Oncology,* 22 (8): 1138–1149. *IF 10.2*

Eismann B*, Krieger TG*, Beneke J, Bulkescher R, Adam L, Erfle H, Herrmann C, Eils R, Conrad C: Automated screening by 3D light-sheet microscopy with high spatial and temporal resolution reveals mitotic phenotypes. *Journal of Cell Science,* 133: jcs245043. *IF 4.6*

2019 Tirier SM, Park J, Preusser F, Amrhein L, Gu Z, Steiger S, Mallm JP, Krieger TG, Waschow M, Eismann B, Gut M, Gut I, Rippe K, Schlesner M, Theis F, Fuchs C, Ball CR, Glimm H, Eils R, Conrad C: pheno-seq - linking visual features and gene expression in 3D cell culture systems. *Scientific Reports*, 9: 12367. *IF 4.1*

Krieger TG, Moran CM, Frangini A, Visser WE, Schoenmakers E, Muntoni F, Clark CA, Gadian D, Chong WK, Kuczynski A, Dattani M, Lyons G, Efthymiadou A, Varga-Khadem F, Simons BD, Chatterjee K, Livesey FJ: Mutations in thyroid hormone receptor α1 cause premature neurogenesis and progenitor cell depletion in human cortical development. *PNAS,* 116 (45): 22754-22763. *IF 9.4*

2018 Basak O, Krieger TG, Muraro MJ, Wiebrands K, Stange DE, Frias-Aldeguer J, Rivron NC, van de Wetering M, van Es JH, van Oudenaarden A, Simons BD, Clevers H: Troy^{+} brain stem cells cycle through quiescence and regulate their number by sensing niche occupancy. *PNAS,* 115 (4): E610-E619. *IF 9.8*

2015 Krieger TG, Simons BD: Dynamic stem cell heterogeneity. Development, 142: 1396-1406. *IF 6.6*

2014 Gao P*, Postiglione MP*, Krieger TG, Wang C, Han Z, Hernandez L, Streicher C, Papusheva E, Insolera R, Kodish O, Simons BD, Huang K, Luo L, Hippenmeyer S, Shi SH: Deterministic progenitor behavior and unitary production of neurons in the neocortex. *Cell,* 159 (4): 775-788. *IF 27.8*

12 Danksagung

Mein Dank gilt Prof. Christian Conrad und Prof. Roland Eils, die die Durchführung dieses Projekts ermöglicht und mich in den vergangenen Jahren in vielfältiger Weise unterstützt haben.

Ich danke auch meinen Kollegen Dr. Jeongbin Park, Dr. Heike Peterziel, Dr. Tanja Eisemann und Prof. Peter Angel, die Proben zur Verfügung gestellt oder durch ihre direkte Mitarbeit zum Gelingen dieses Projekts beigetragen haben.

Den gegenwärtigen und ehemaligen Mitgliedern meiner Arbeitsgruppe, insbesondere Dr. Marcel Waschow, Dr. Björn Eismann, Dr. Stephan Tirier, Dr. Julia Jabs und Dr. Luca Tosti, danke ich für erhellende wissenschaftliche und weniger wissenschaftliche Diskussionen, den Kaffee und heitere Stunden auch außerhalb des Labors.

Ganz besonders danke ich meiner Familie für ihre liebevolle Unterstützung.